Superscaling analyses, lepton scattering and nucleon momentum distribution in nuclei

A.N. Antonov[1]   M.V. Ivanov[1]   M.K. Gaidarov[1]
J.A. Caballero[2]   M.B. Barbaro[3]   E. Moya de Guerra[4]

[1]Institute for Nuclear Research and Nuclear Energy,
Bulgarian Academy of Sciences, Sofia, Bulgaria

[2]Departamento de Física Atómica, Molecular y Nuclear, Universidad de Sevilla,
Sevilla, Spain

[3]Dipartimento di Fisica Teorica, Università di Torino and INFN, Sezione di Torino,
Torino, Italy

[4]Departamento de Fisica Atomica, Molecular y Nuclear, Facultad de Ciencias
Fisicas, Universidad Complutense de Madrid, Madrid, Spain

Inclusive electron scattering (e, e')

$$\vec{q} = \vec{p_e} - \vec{p_{e'}},$$
$$\omega = T_e - T_{e'},$$

momentum and energy transferred by the probe to the constituent of the composite system.

At larger energy loss, a broad peak due to quasi-elastic electron-nucleon scattering appears; this peak - very wide due to nuclear Fermi motion - corresponds to processes where the electron scatters from an individual, moving nucleon, which, after interaction with other nucleons, is ejected from the target.
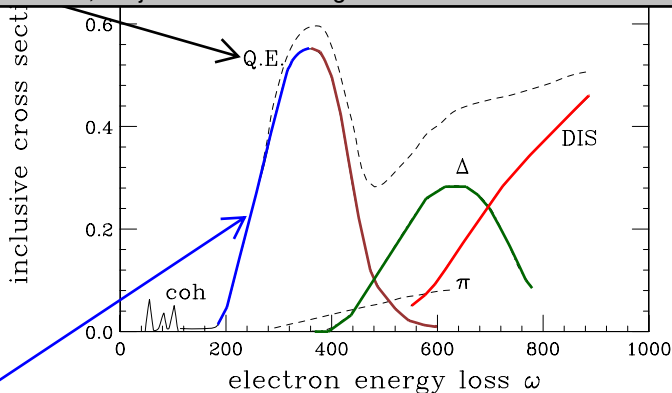
One finds that in the relevant energy range in the region below the QE peak scaling of the second kind is found to be excellent and scaling of the first kind to be quite good.

Relativistic Fermi Gas (RFG) (without interaction between the nucleons)
Dimensionless scaling variable ψ':

$$\psi' = \frac{1}{\sqrt{\xi_F}} \frac{\lambda' - \tau'}{\sqrt{(1 + \lambda')\tau' + \kappa\sqrt{\tau'(1 + \tau')}}}. \tag{1}$$

k_F – Fermi momentum; $\eta_F = k_F/m_N$ – dimensionless Fermi momentum;
$\xi_F = \sqrt{1 + \eta_F^2} - 1$ – dimensionless Fermi kinetic energy

$\kappa \equiv \dfrac{q}{2m_N}; \quad \lambda' \equiv \dfrac{\omega'}{2m_N}, \quad \omega' \equiv \omega - E_{shift};$

$\tau' \equiv \dfrac{|Q^2|}{4m_N^2} = \kappa^2 - \lambda'^2$ – dimensionless absolute value of the

squared 4–transferred momentum
The physical meaning of ψ'^2 (in units of the Fermi energy) is the
smallest kinetic energy that one of the nucleons responding to an
external probe can have.

$$F(\kappa, \psi') \equiv \frac{d^2\sigma/d\Omega_e d\omega'}{\sigma_M[v_L G_L(\kappa, \lambda') + v_T G_T(\kappa, \lambda')]} \qquad (2)$$

σ_M – Mott cross section; $d^2\sigma/d\Omega_e d\omega'$ – the cross section of the inclusive electron scattering; v_L, v_T – Rosenbluth lepton kinematical factors; G_L, G_T – single-nucleon responses expressed by Sachs form factors, functions of τ', $G_{E_{p,n}}$ and $G_{M_{p,n}}$.

In the RFG model:

$$F^{\mathrm{RFG}} = F_T^{\mathrm{RFG}} = F_L^{\mathrm{RFG}}. \qquad (3)$$

Dimensionless scaling function:

$$f_{\mathrm{RFG}}(\psi') = k_F \cdot F^{\mathrm{RFG}}(\psi') \underset{(\eta_F^2 \ll 1)}{\simeq} \frac{3}{4}(1-\psi'^2)\Theta(1-\psi'^2) \qquad (4)$$

📄 M. Barbaro *et al.*, *Nucl. Phys. A* **643**, 137 (1998).

At sufficiently high energies > 500 MeV:

- When $f(\psi')$ depends only on ψ' and not on the momentum transfer q one has **scaling of the first kind**.
- When $f(\psi')$ and ψ' are independent of the mass number A for a wide range of nuclei from ^{4}He to ^{197}Au, one has **scaling of the second kind**.

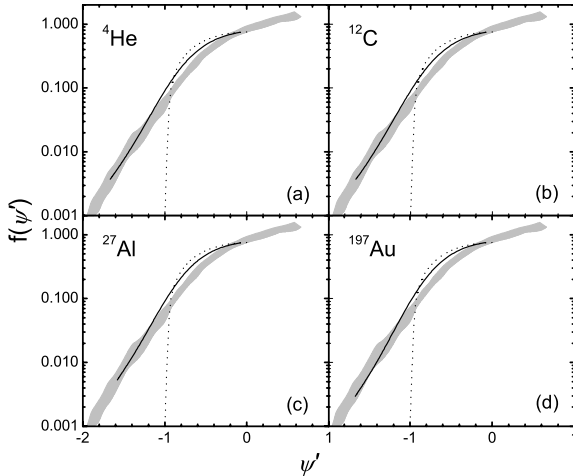When both types of scaling occur one says that a scaling function exhibits **superscaling**.

Figure: Scaling function $f(\psi')$ in the CDFM (solid line) at $q = 1560$ MeV/c for ^{4}He, ^{12}C, ^{27}Al, and ^{197}Au. The experimental data are given by the shaded area. The RFG result is shown by dotted line.

Thus, it became necessary to consider the superscaling in theoretical methods which go beyond the RFG. One of them is the Coherent Density Fluctuation Model (CDFM) that is a natural extension of the Fermi gas case to realistic finite nuclear system beyond the mean field approximation. The accounting for NN correlations in CDFM in the momentum and density distribution made it possible to reproduce the available experimental data for $\psi' < 0$, including $\psi' \lesssim -1$.

📄 A. N. Antonov, V. A. Nikolaev, and I. Zh. Petkov, *Bulg. J. Phys.* **6**, 151 (1979); *Z. Phys. A* **297**, 257 (1980); *ibid.* **304**, 239 (1982); *Nuovo Cimento A* **86**, 23 (1985).

📄 A. N. Antonov, P. E. Hodgson, and I. Zh. Petkov, *Nucleon Momentum and Density Distributions in Nuclei* (Clarendon Press, Oxford, 1988); *Nucleon Correlations in Nuclei* (Springer-Verlag, Berlin-Heidelberg-New York, 1993).

📄 A.N. Antonov, M.K. Gaidarov *et al.*, *Phys. Rev. C* **69**, 044321 (2004); *Phys. Rev. C* **71**, 014317 (2005), *Phys. Rev. C* **73**, 047302 (2006).

The hard-sphere dilute Fermi gas (HSDFG) is a low density gas of fermions that interact via a repulsive hard-core potential.

A. B. Migdal, *Zh. Eksp. Teor. Fiz.* **32**, 333 (1957);
V. M. Galitskii, *Zh. Eksp. Teor. Fiz.* **34**, 151 (1958);
V. A. Belyakov, *Zh. Eksp. Teor. Fiz.* **40**, 1210 (1961);
W. Czyż and K. Gottfried, *Nucl. Phys.* **21**, 676 (1961);
R. Sartor and C. Mahaux, *Phys. Rev. C* **21**, 1546 (1980);
Phys. Rev. C **25**, 677 (1982).

In the HSDFG, as shown by Migdal $n(k)$ in the normal Fermi gas is discontinuous at the Fermi momentum $k = k_F$. This discontinuity is an inherent consequence of an arbitrary interaction between particles in an infinite system.
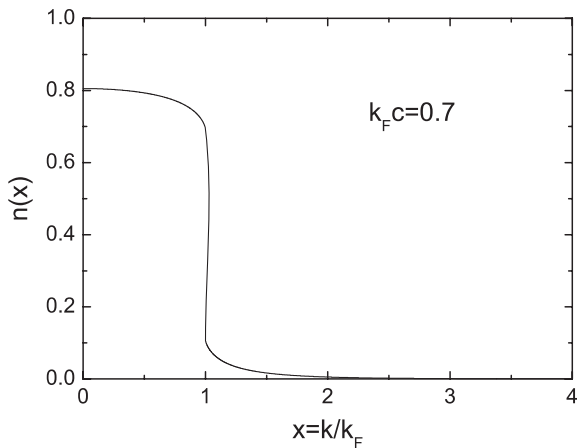
Figure: The momentum distribution $n(k)$ in hard-sphere dilute Fermi gas as a function of $x = k/k_F$ ($c = 0.50$ fm, $k_F = 1.40$ fm^{-1}).

$$f^{\mathsf{HSDFG}}(\psi') \simeq \frac{3}{2} \int\limits_{|\psi'|}^{\infty} x n(x) dx, \ \left[\text{at} \ \left(\frac{k_F}{m_N}\right)^2 \ll 1\right]. \qquad (1)$$

It follows from Eq. (1) that the HSDFG system also exhibits superscaling.

General consideration of the asymptotic behavior of $n(k)$ in:

📄 R. D. Amado and R. M. Woloshyn, *Phys. Lett. B* **62**, 253 (1976);
📄 R. D. Amado, *Phys. Rev. C* **14**, 1264 (1976);
📄 R. D. Amado and R. M. Woloshyn, *Phys. Rev. C* **15**, 2200 (1977).

At large k, $n(k)$ has a power-law decrease

$$n(k) \xrightarrow[k\to\infty]{} \left[\frac{\widetilde{V}_{NN}(k)}{k^2} \right]^2. \tag{2}$$

$\widetilde{V}_{NN}(k)$ is the Fourier transform of the NN interaction $V_{NN}(r)$.
For δ-forces (as in the HSDFG):

$$n(k) \sim 1/k^4$$

Under question: k or k/A must be large for Eq. (2) to apply?
Typically $n(k) \sim 1/k^{4+m}$, $m > 0$ (*i.e.* $\widetilde{V}_{NN}(k) \sim \dfrac{1}{k^{m/2}}$).

For $k < k_F$: $n(k)$ from HSDFG.

$$\text{For } k > k_F: n(k) \sim \frac{1}{k^{4+m}}, \ (k_F c = 0.70). \tag{3}$$

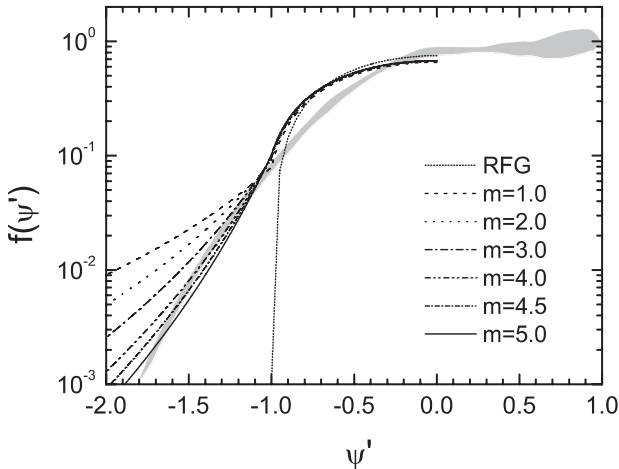$$f(\psi') = 0.12\left(\frac{1+m}{2+m}\right)\frac{1}{|\psi'|^{2+m}}. \tag{4}$$

Figure: The scaling function in a dilute Fermi gas for different values of m in the asymptotics of the momentum distribution $n(k) \sim 1/k^{4+m}$ given in comparison with the RFG result. The grey area shows experimental data.

Agreement with the experimental QE scaling function is achieved when $\boxed{m \simeq 4 \div 5}$ in Eqs. (3) and (4), i.e.

$$n(k) \underset{(k \to \infty)}{\sim} \frac{1}{k^8} \div \frac{1}{k^{10}}. \tag{5}$$

In CDFM:

$$n(k) \sim \frac{1}{k^8}, \tag{6}$$

i.e. $n(k) \sim 1/k^{4+m}$ with $\boxed{m = 4}$.
The inverse Fourier transform gives

$$V_{NN}(r) \sim \frac{1}{r} \text{ for } m = 4; \qquad V_{NN}(r) \sim \frac{1}{r^{1/2}} \text{ for } m = 5.$$

The behavior of the QE scaling function depends mainly on the particular form of the power-law asymptotics of $n(k)$.

📄 A.N. Antonov, M.V. Ivanov, M.K. Gaidarov, E. Moya de Guerra, *Phys. Rev. C* **75**, 034319 (2007).

3.1 CDFM (first approach)

The Wigner distribution function which corresponds to the ODM

$$
W(\mathbf{r}, \mathbf{k}) = \frac{4}{(2\pi)^3} \int\limits_0^\infty dx |F(x)|^2 \Theta(x - |\mathbf{r}|)\Theta(k_F(x) - |\mathbf{k}|) \qquad (1)
$$

$$
\rho(\mathbf{r}) = \int d\mathbf{k}\, W(\mathbf{r}, \mathbf{k}) = \int\limits_0^\infty dx |F(x)|^2 \frac{3A}{4\pi x^3}\Theta(x - |\mathbf{r}|), \qquad (2)
$$

$$
n(\mathbf{k}) = \int d\mathbf{r}\, W(\mathbf{r}, \mathbf{k}) = \frac{4}{(2\pi)^3} \int\limits_0^\infty dx |F(x)|^2 \frac{4\pi x^3}{3}\Theta(k_F(x) - |\mathbf{k}|)
$$

$$
= \frac{4}{(2\pi)^3} \int\limits_0^{\alpha/k} dx |F(x)|^2 \frac{4}{3}\pi x^3, \quad (3)
$$

$$k_F(x) = \left(\frac{3\pi^2}{2}\rho_0(x)\right)^{1/3} \equiv \frac{\alpha}{x} \text{ with } \alpha = \left(\frac{9\pi A}{8}\right)^{1/3} \simeq 1.52 A^{1/3}, \quad (4)$$

where x is the radius of a sphere of nuclear matter containing A nucleons.

$$|\mathcal{F}(x)|^2 = -\frac{1}{\rho_0(x)} \left.\frac{d\rho(r)}{dr}\right|_{r=x} \text{ at } \frac{d\rho(r)}{dr} \leq 0 \quad (5)$$

$$|\mathcal{F}(x)|^2 = -\frac{3\pi^2}{2}\frac{\alpha}{x^5} \left.\frac{dn(k)}{dk}\right|_{k=\frac{\alpha}{x}} \text{ at } \frac{dn(k)}{dk} \leq 0 \quad (6)$$

$$\int \rho(\mathbf{r})d\mathbf{r} = A; \quad \int n(\mathbf{k})d\mathbf{k} = A \quad (7)$$

$$\int\limits_0^\infty |F(x)|^2 dx = 1 \quad (8)$$

Our basic assumption within the CDFM is that the scaling function for a finite nucleus $f(\psi')$ can be defined by means of the weight function $|F(x)|$, weighting the scaling function for the RFG at given x.

$$f(\psi') = \int\limits_{0}^{\alpha/(k_F|\psi'|)} |\mathcal{F}(x)|^2 f_{\text{RFG}}(\psi', x) dx \qquad (9)$$

$$f(\psi') = \frac{4\pi}{A} \int\limits_{0}^{\alpha/(k_F|\psi'|)} \rho(x) \left[x^2 f_{\text{RFG}}(\psi', x) + \frac{x^3}{3} \frac{df_{\text{RFG}}(\psi', x)}{dx} \right] dx \qquad (10)$$

$$f(\psi') = \frac{4\pi}{A} \int\limits_{k_F|\psi'|}^{\infty} n(k) \left[k^2 f_{\text{RFG}}(\psi', k) + \frac{k^3}{3} \frac{df_{\text{RFG}}(\psi', k)}{dk} \right] dk \qquad (11)$$

$$\lim_{k \to \infty} n(k)k^3 = 0$$

$$k_F = \int\limits_{0}^{\infty} |F(x)|^2 \frac{\alpha}{x} dx. \qquad (12)$$

3.2 CDFM (second approach)

Hadronic tensor in the CDFM$_{\mathrm{II}}$:

$$W^{\mu\nu}_{\mathrm{CDFM}} = \int\limits_0^\infty |F(x)|^2 W^{\mu\nu}_{\mathrm{(RFG)}}(x)dx. \tag{1}$$

Responses with longitudinal projections:

$$R_L(\psi) = \int\limits_0^\infty R_L(x,\psi)|F(x)|^2 dx, \ R_L(x,\psi) = R_{L,p}(x,\psi) + R_{L,n}(x,\psi). \tag{2}$$

Responses with transverse projections:

$$R_T(\psi) = \int\limits_0^\infty R_T(x,\psi)|F(x)|^2 dx, \ R_T(x,\psi) = R_{T,p}(x,\psi) + R_{T,n}(x,\psi). \tag{3}$$

$$Q^2 = \omega^2 - q^2 \leq 0$$

$$R_{L,n(p)}(x,\psi) = \frac{3N(Z)}{4m_N\kappa\eta_F^3(x)}(\varepsilon_F(x) - \Gamma(x))\Theta(\varepsilon_F(x) - \Gamma(x))\times$$

$$\times\frac{\kappa^2}{\tau}\left[(1+\tau)W_{2,n(p)}(\tau) - W_{1,n(p)}(\tau) + W_{2,n(p)}(\tau)\Delta(x,\psi)\right]; \quad (4)$$

$$R_{T,n(p)}(x,\psi) = \frac{3N(Z)}{4m_N\kappa\eta_F^3(x)}(\varepsilon_F(x) - \Gamma(x))\Theta(\varepsilon_F(x) - \Gamma(x))\times$$

$$\times\left[2W_{1,n(p)}(\tau) + W_{2,n(p)}(\tau)\Delta(x,\psi)\right], \quad (5)$$

where

$$\Delta(x,\psi) = \frac{\tau}{\kappa^2}\Big[\frac{1}{3}(\varepsilon_F^2(x) + \varepsilon_F(x)\Gamma(x) + \Gamma^2(x)) +$$

$$+ \lambda(\varepsilon_F(x) + \Gamma(x)) + \lambda^2\Big] - (1+\tau) \quad (6)$$

with

$$\Gamma(x) \equiv \max\left[(\varepsilon_F(x) - 2\lambda), \gamma_- \equiv \kappa\sqrt{1 + \frac{1}{\tau}} - \lambda\right] \quad (7)$$

and

$$W_{1,p}(\tau) = \tau G_{M,p}^2(\tau), \ W_{1,n}(\tau) = \tau G_{M,n}^2(\tau) \tag{8}$$

$$W_{2,p}(\tau) = \frac{1}{1+\tau} \left[G_{E,p}^2(\tau) + \tau G_{M,p}^2(\tau) \right] \tag{9}$$

$$W_{2,n}(\tau) = \frac{1}{1+\tau} \left[G_{E,n}^2(\tau) + \tau G_{M,n}^2(\tau) \right]. \tag{10}$$

$$\kappa = q/2m_N, \ \lambda = \omega/2m_N, \ \tau = \kappa^2 - \lambda^2,$$

$$\eta \equiv |\mathbf{p}|/m_N, \ \varepsilon \equiv E(\mathbf{p})/m_N = \sqrt{1+\eta^2}, \tag{11}$$

$$\eta_F(x) = \frac{k_F(x)}{m_N} = \frac{\alpha}{x m_N}, \ \varepsilon_F(x) = \sqrt{1+\eta_F^2(x)} = \sqrt{1+\left(\frac{\alpha}{x m_N}\right)^2} \tag{12}$$

We label $\dfrac{d^2\sigma}{d\Omega d\varepsilon'}$ by $C^{\mathrm{CDFM}}(\psi)$:

$$C^{\mathrm{CDFM}}(\psi) \equiv \frac{d^2\sigma}{d\Omega d\varepsilon'} =$$

$$= \sigma_M \left\{ \left(\frac{Q^2}{q^2}\right)^2 R_L(\psi) + \left[\frac{1}{2}\left|\frac{Q^2}{q^2}\right| + \tan^2\frac{\theta}{2}\right] R_T(\psi) \right\}. \tag{13}$$

Single-nucleon eN elastic cross section:

$$S^{\text{QE}} = \sigma_M \left\{ \left(\frac{Q^2}{q^2} \right)^2 G_L^{\text{QE}}(\tau) + \left[\frac{1}{2} \left| \frac{Q^2}{q^2} \right| + \tan^2 \frac{\theta}{2} \right] G_T^{\text{QE}}(\tau) \right\}, \quad (14)$$

where single-nucleon functions G_L and G_T are given by:

$$G_L^{\text{QE}}(\tau) = \frac{\kappa}{2\tau} [Z G_{E,p}^2(\tau) + N G_{E,n}^2(\tau)] + \mathcal{O}(\eta_F^2) \quad (15)$$

$$G_T^{\text{QE}}(\tau) = \frac{\tau}{\kappa} [Z G_{M,p}^2(\tau) + N G_{M,n}^2(\tau)] + \mathcal{O}(\eta_F^2). \quad (16)$$

Superscaling function is evaluated by

$$f_{\text{CDFM}}(\psi) = k_F \times \frac{C^{\text{CDFM}}(\psi)}{S^{\text{QE}}}, \quad (17)$$

and longitudinal L and transverse T scaling functions are introduced:

$$f_L(\psi) = k_F \times \frac{R_L(\psi)}{G_L^{\text{QE}}}, \qquad f_T(\psi) = k_F \times \frac{R_T(\psi)}{G_T^{\text{QE}}}. \quad (18)$$
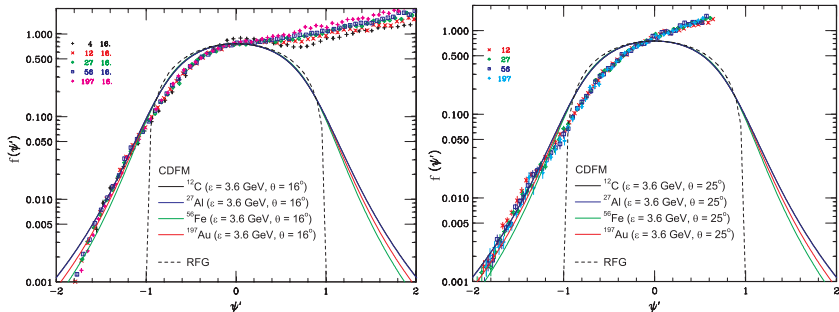
Figure: The quasielastic scaling function $f^{QE}(\psi')$ for ^{12}C, ^{27}Al, ^{56}Fe, and ^{197}Au calculated in the CDFM$_I$. The experimental data are taken from T. W. Donnelly and I. Sick, *Phys. Rev. Lett.* **82**, 3212 (1999); *Phys. Rev. C* **60** (1999) 065502.
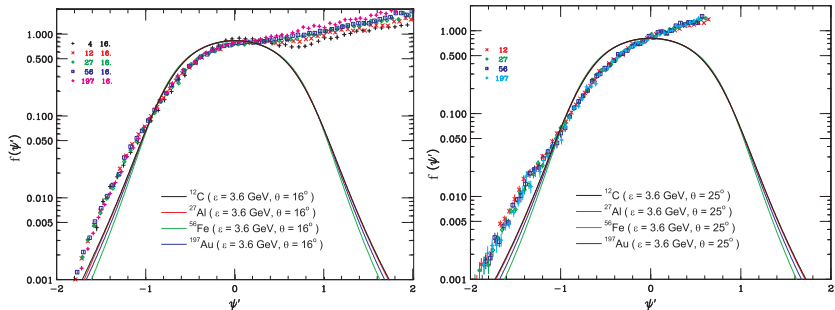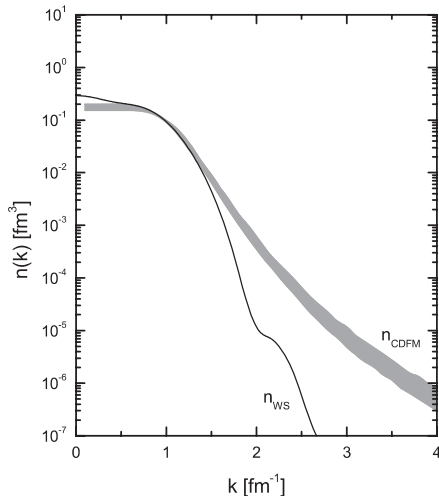
Figure: The quasielastic scaling function $f^{QE}(\psi')$ for ^{12}C, ^{27}Al, ^{56}Fe, and ^{197}Au calculated in the CDFM$_{II}$. The experimental data are taken from T. W. Donnelly and I. Sick, *Phys. Rev. Lett.* **82**, 3212 (1999); *Phys. Rev. C* **60** (1999) 065502.

Figure: The nucleon momentum distribution $n(k)$. Gray area: combined results of CDFM for ^{4}He, ^{12}C, ^{27}Al, ^{56}Fe and ^{197}Au. Solid line: mean-field result using Woods-Saxon single-particle wave functions (for ^{56}Fe). The normalization is: $\int n(k) d^3 k = 1$.
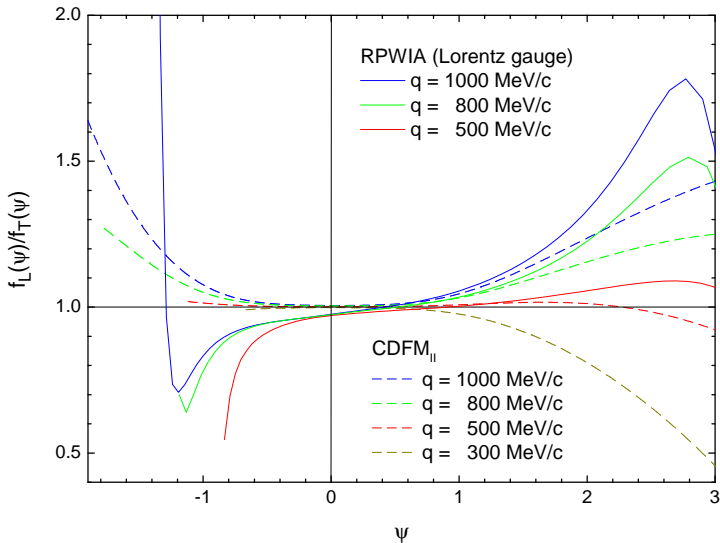
Figure: The ratio $f_L(\psi)/f_T(\psi)$ for ^{12}C calculated in the CDFM$_{II}$ and RPWIA (Lorentz gauge) for $q = 300$, 500, 800, and 1000 MeV/c.
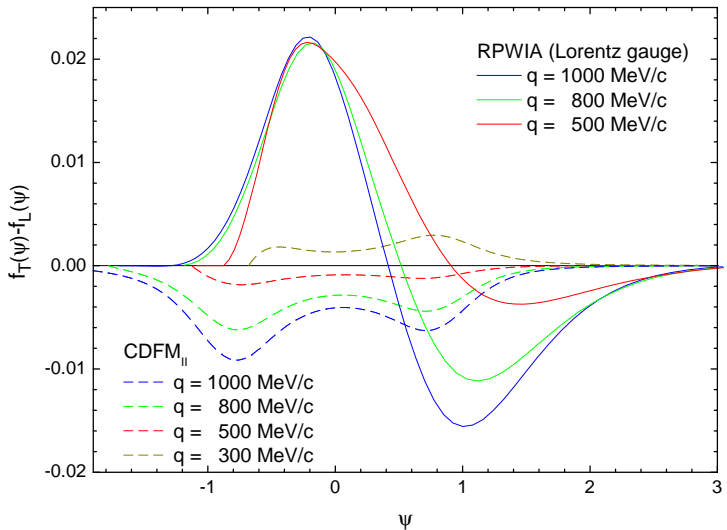
Figure: The differences $f_T(\psi) - f_L(\psi)$ for ^{12}C calculated in the CDFM$_{\parallel}$ and RPWIA (Lorentz gauge) for $q = 300$, 500, 800, and 1000 MeV/c.
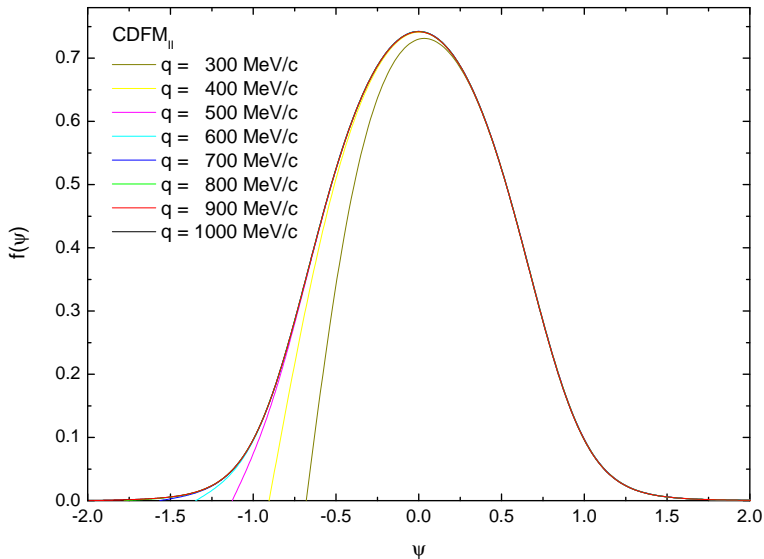
Figure: The quasielastic scaling function $f^{QE}(\psi')$ for ^{12}C calculated in the $CDFM_{II}$ for $q = 300 - 1000$ MeV/c with step 100 MeV/c .
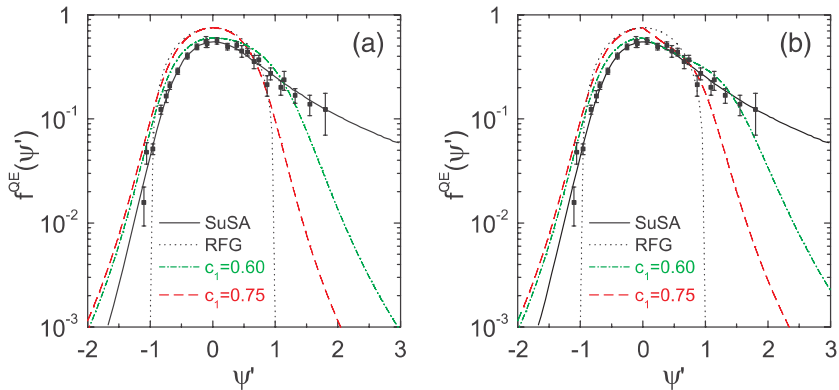
Figure: The quasielastic scaling function $f^{QE}(\psi')$ for ^{12}C calculated in the CDFM using parabolic form (a) and exponential form (b).
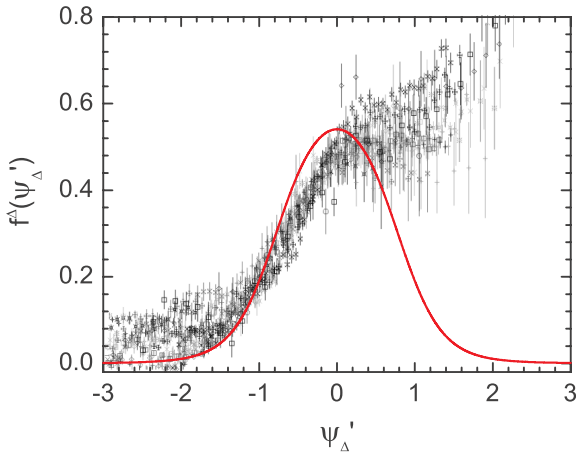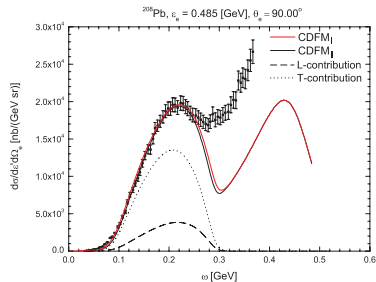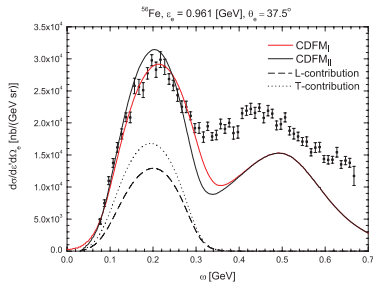
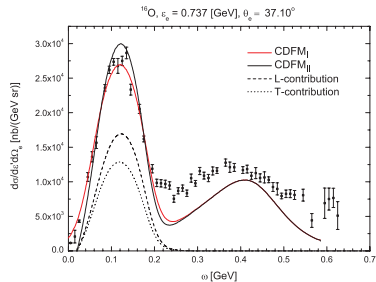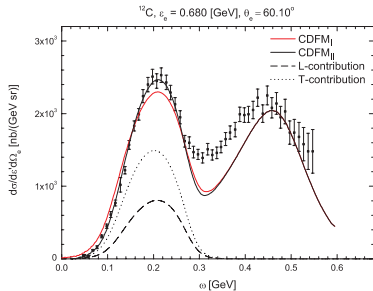Figure: The CDFM scaling function $f^{\Delta}(\psi'_{\Delta})$ in the Δ-region (solid red line). Averaged experimental values of $f^{\Delta}(\psi'_{\Delta})$ are taken from: J. E. Amaro, M. B. Barbaro, J. A. Caballero, T. W. Donnelly, A. Molinari, and I. Sick, *Phys. Rev. C* **71**, 015501 (2005).

– Following:

📄 J. E. Amaro, M. B. Barbaro, J. A. Caballero, T. W. Donnelly, A. Molinari, and I. Sick, *Phys. Rev. C* **71**, 015501 (2005).

the CC neutrino cross section in the target laboratory frame is given in the form

$$\left[\frac{d^2\sigma}{d\Omega dk'} \right]_\chi \equiv \sigma_0 \mathcal{F}_\chi^2, \tag{1}$$

where $\chi = +$ for neutrino-induced reactions (for example, $\nu_l + n \rightarrow \ell^- + p$, where $\ell = e, \mu, \tau$) and $\chi = -$ for antineutrino-induced reactions (for example, $\overline{\nu_l} + p \rightarrow \ell^+ + n$),

$$\sigma_0 \equiv \frac{(G \cos\theta_c)^2}{2\pi^2} \left[k' \cos\widetilde{\theta}/2 \right]^2, \tag{2}$$

where $G = 1.16639 \times 10^{-5}$ GeV^{-2} is the Fermi constant, θ_c is the Cabibbo angle ($\cos\theta_c = 0.9741$),

$$\tan^2\widetilde{\theta}/2 \equiv \frac{|Q^2|}{v_0}, \ v_0 \equiv (\epsilon + \epsilon')^2 - q^2 = 4\epsilon\epsilon' - |Q^2|. \tag{3}$$

Instead of the RFG scaling functions in the QE and Δ regions, we use those obtained in the CDFM.
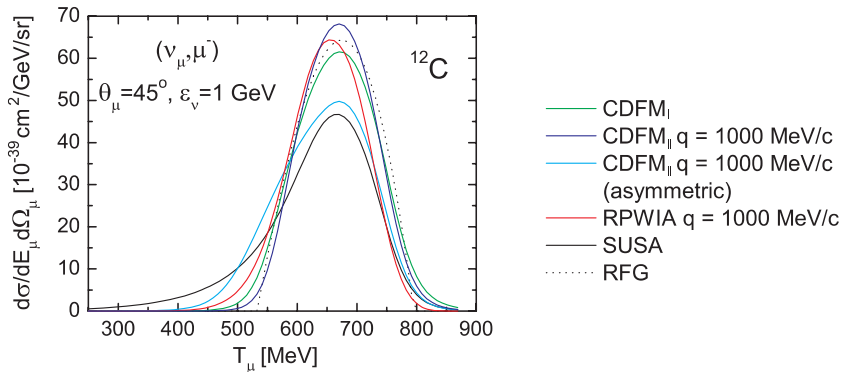
Figure: The cross section of charge-changing neutrino (ν_μ, μ^-) reaction on ^{12}C at $\theta_\mu = 45°$ and $\varepsilon_\nu = 1$ GeV.

Figure: The cross section of charge-changing neutrino (ν_μ,μ^-) reaction on ^{12}C at $\theta_\mu = 30°$ and $\varepsilon_\nu = 1$ GeV. (a) QE contributions: solid line: the result of CDFM with $c_1 = 0.63$; dashed line: CDFM with $c_1 = 0.72$; dotted line: RFG; dot-dashed line: SuSA result; double dot-dashed line: the result for the Δ-contribution from the CDFM. (b) the sum of QE- and Δ-contributions in RFG model (dotted line), in the CDFM with $c_1 = 0.63$ (solid line) and $c_1 = 0.72$ (dashed line).

Figure: The cross section of charge-changing neutrino (ν_μ, μ^-) reaction on ^{12}C at $\theta_\mu = 45°$ and $\varepsilon_\nu = 1$ GeV.

Figure: The cross section of charge-changing neutrino (ν_μ, μ^-) reaction on ^{12}C at $\theta_\mu = 60°$ and $\varepsilon_\nu = 1$ GeV.
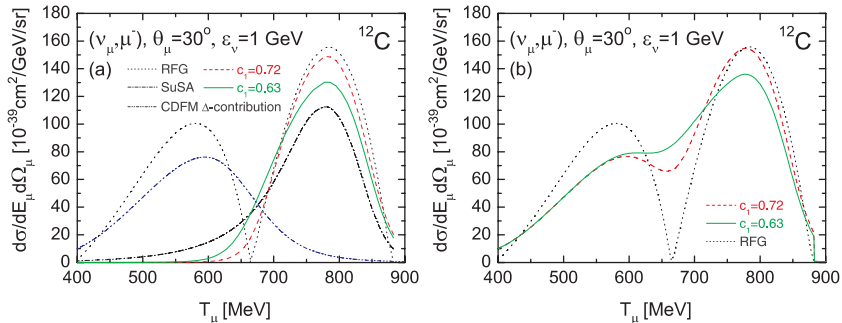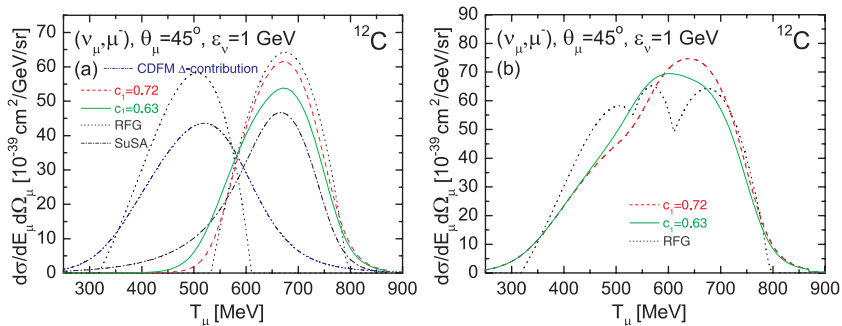
Figure: The cross section of charge-changing neutrino (ν_μ, μ^-) reaction on ^{12}C at $\theta_\mu = 45^\circ$ and $\varepsilon_\nu = 1.5$ GeV.
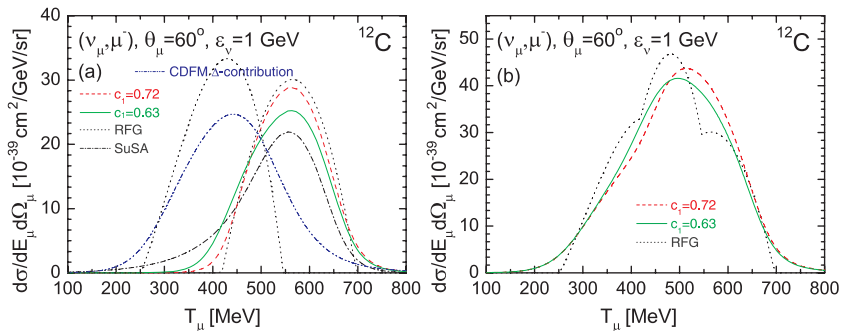
Figure: The cross section of charge-changing neutrino (ν_μ,μ^-) reaction on ^{12}C at $\theta_\mu = 45°$ and $\varepsilon_\nu = 2$ GeV.
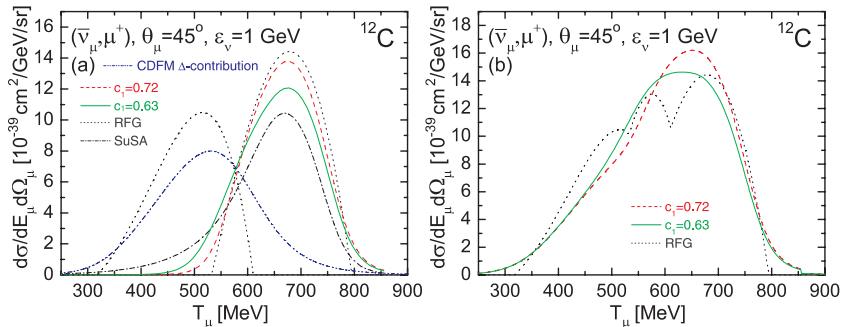
Figure: The cross section of charge-changing antineutrino ($\overline{\nu}_\mu, \mu^+$) reaction on ^{12}C at $\theta_\mu = 45°$ and $\varepsilon_{\overline{\nu}} = 1$ GeV.

A.N. Antonov, M.V. Ivanov *et al.*, *Phys. Rev. C* **74**, 054603 (2006); *Phys. Rev. C* **75**, 064617 (2007); *Phys. Rev. C* **77**, 034612 (2008); *Phys. Rev. C* **79**, 044602 (2009).

Following procedure for calculating the inclusive cross section in the u-channel from work:

📄 J. E. Amaro, M. B. Barbaro, J. A. Caballero, and T. W. Donnelly, Phys. Rev. C **73**, 035503 (2006) – SuperScaling Analysis (SuSA).

The RFG scaling function is found to be:

$$F_{\text{RFG}}(\psi_{\text{RFG}}^{(u)}) = \frac{3}{4} k_F \left(1 - \psi_{\text{RFG}}^{(u)2}\right) \Theta \left(1 - \psi_{\text{RFG}}^{(u)2}\right). \qquad (1)$$

We weight the $F_{\text{RFG}}(\psi_{\text{RFG}}^{(u)})$ by means of the CDFM function $|F(x)|^2$.

📄 A.N. Antonov, M.V. Ivanov, M.B. Barbaro, J.A. Caballero, E. Moya de Guerra, and M. K. Gaidarov, *Phys. Rev. C* **75**, 064617 (2007).
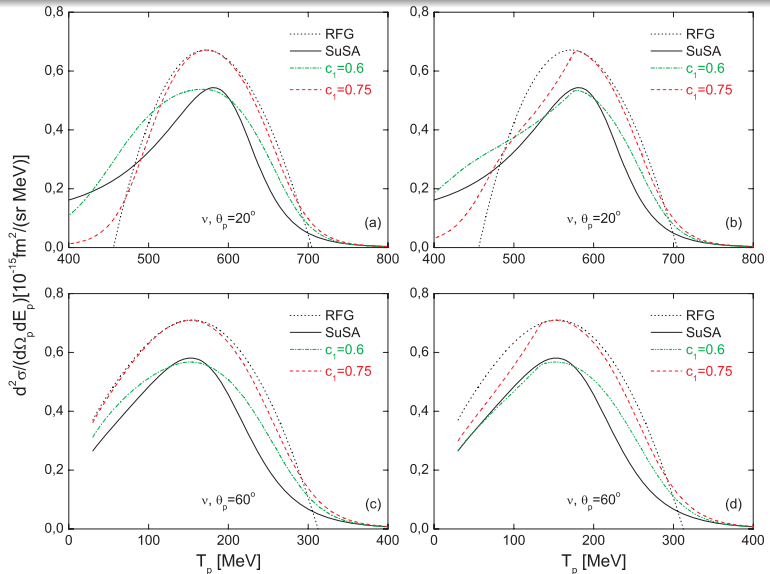
Figure: Quasielastic differential cross section for neutral current neutrino scattering at 1 GeV from ^{12}C for proton knockout at $\theta_p = 20°$ (a,b) and $60°$ (c,d).

Figure: Quasielastic differential cross section for neutral current antineutrino scattering at 1 GeV from ^{12}C for proton knockout.

Figure: Quasielastic differential cross section for neutral current neutrino scattering at 1 GeV from ^{12}C for neutron knockout.

Figure: Quasielastic differential cross section for neutral current antineutrino scattering at 1 GeV from ^{12}C for neutron knockout.

<u>Conclusions:</u>

1. It is pointed out that $f(\psi')$ for $\psi' < -1$ depends on the <u>particular form of the power-law asymptotics</u> of $n(k)$ at large k and thus, is informative for the <u>in-medium NN forces</u> around the core.
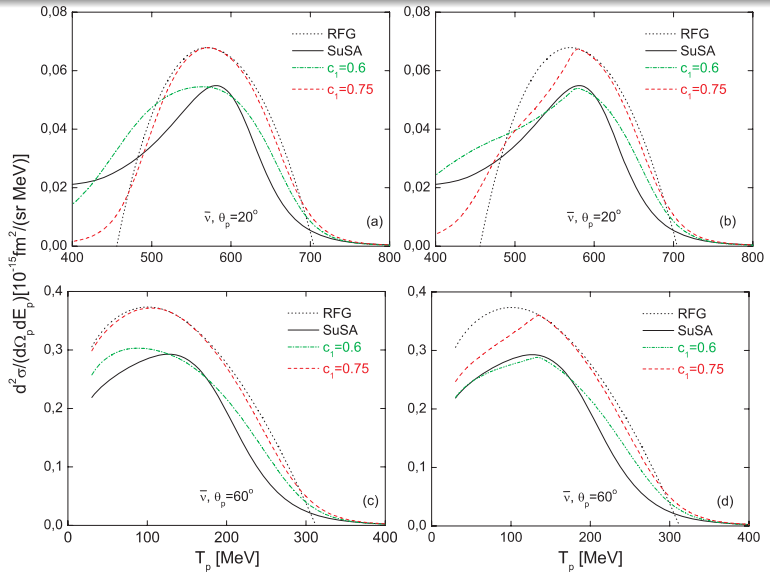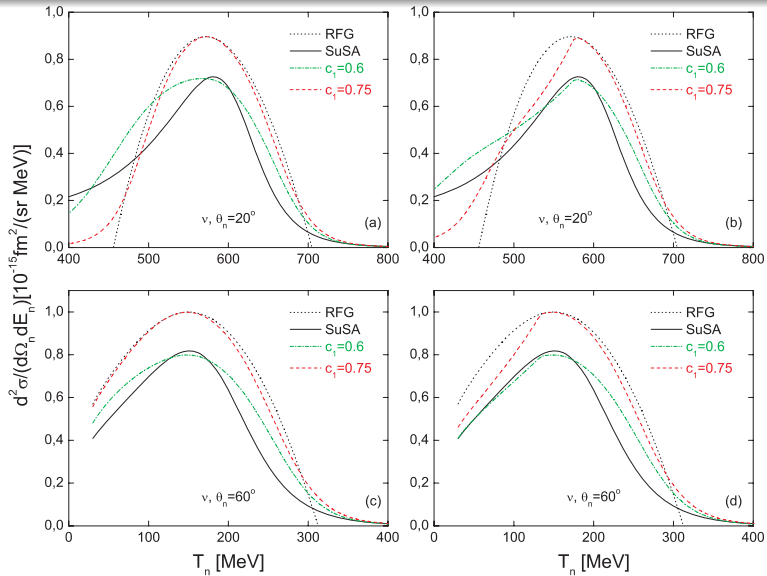
2. The total $f(\psi)$, the longitudinal $f_L(\psi)$ and the transverse $f_T(\psi)$ scaling functions are calculated within a new, more general approach within the Coherent Density Fluctuation Model (CDFM$_{II}$) by taking as starting point the hadronic tensor and the L- and T- response functions in the RFG model.

3. The approach leads to a slight violation of the zero-kind scaling $[f_L(\psi) \neq f_T(\psi)]$ in contrast with the situation in the RFG and CDFM$_I$ models. It is found that the ratio $f_L(\psi)/f_T(\psi)$ in the CDFM$_{II}$ has similarities with that from the RPWIA approach (with Lorentz gauge) for positive ψ.

4. At $q \gtrsim 0.7$ GeV/c the CDFM$_{II}$ scaling function exhibits scaling of first kind and has a saturation of its asymptotic behavior.

5. The CDFM scaling functions are applied to calculate cross sections of inclusive electron scattering in the quasielastic and Δ-regions for nuclei with $12 \leq A \leq 208$ at different energies and angles. The results are in agreement with available experimental data, especially in the QE region.

6. The CDFM scaling functions are applied to calculate charge-changing neutrino (antineutrino) scattering and also QE scattering via the weak neutral current on ^{12}C at $1 \div 2$ GeV incident energy.

Superscaling analyses, lepton scattering and nucleon momentum distribution in nuclei

A.N. Antonov[1]   M.V. Ivanov[1]   M.K. Gaidarov[1]
M.B. Barbaro[2]   J.A. Caballero[3]   E. Moya de Guerra[4,5]
P. Sarriguren[4]   J.M. Udias[5]

[1]Institute for Nuclear Research and Nuclear Energy,
Bulgarian Academy of Sciences, Sofia, Bulgaria

[2]Dipartimento di Fisica Teorica, Università di Torino and INFN, Sezione di Torino,
Torino, Italy

[3]Departamento de Física Atómica, Molecular y Nuclear, Universidad de Sevilla,
Sevilla, Spain

[4]Instituto de Estructura de la Materia, CSIC, Madrid, Spain

[5]Departamento de Fisica Atomica, Molecular y Nuclear, Facultad de Ciencias
Fisicas, Universidad Complutense de Madrid, Madrid, Spain

Inclusive electron scattering (e, e')

$$\vec{q} = \vec{p_e} - \vec{p_{e'}},$$
$$\omega = T_e - T_{e'},$$

momentum and energy transferred by the probe to the constituent of the composite system.

$\kappa \equiv q/2m_N$ – dimensionless transferred momentum,

$\lambda \equiv \omega/2m_N$ – dimensionless transferred energy,

$\tau \equiv |Q^2|/4m_N^2 = \kappa^2 - \lambda^2$ – dimensionless absolute value of the squared 4-transferred momentum.
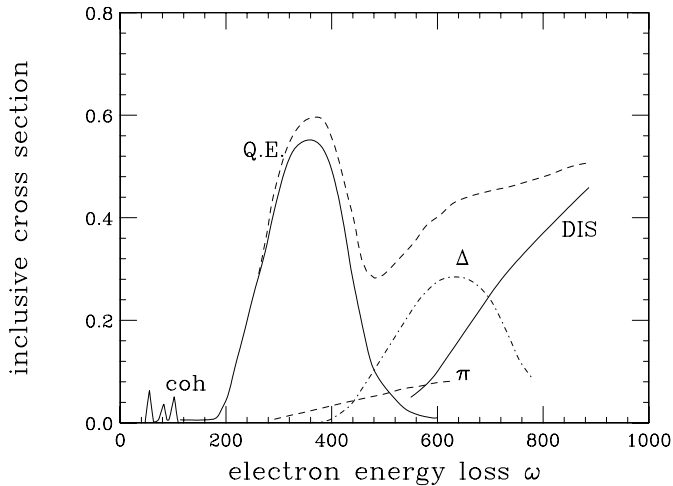
Figure: Schematic representation of inclusive electron cross section as function of energy loss.

At low energy loss peaks due to elastics scattering and inelastic excitation of discrete nuclear states appear.
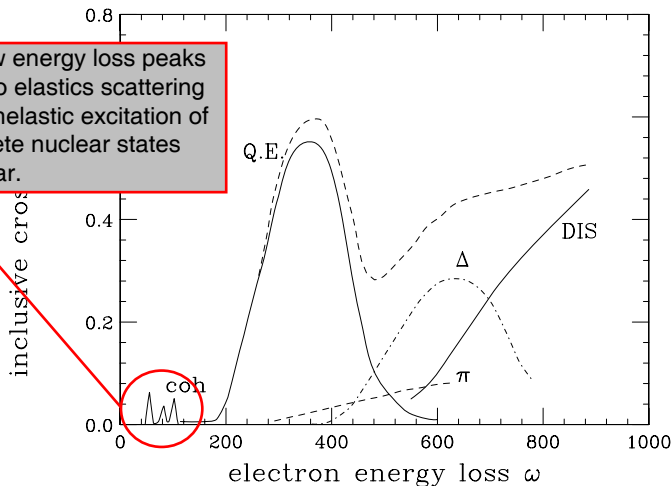
Figure: Schematic representation of inclusive electron cross section as function of energy loss.

At larger energy loss, a broad peak due to quasi-elastic electron-nucleon scattering appears; this peak - very wide due to nuclear Fermi motion - corresponds to processes where the electron scatters from an individual, moving nucleon, which, after interaction with other nucleons, is ejected from the target.
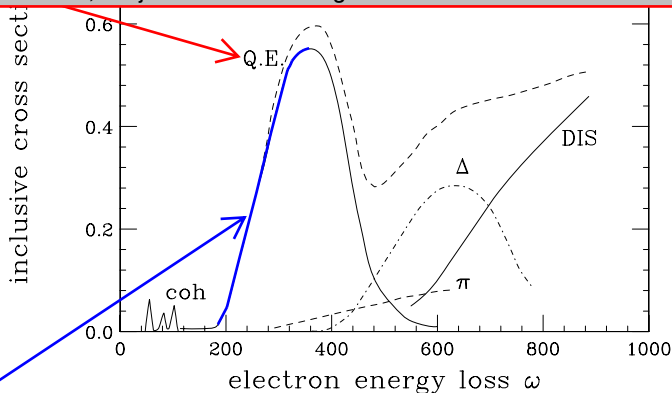
One finds that in the relevant energy range in the region below the QE peak scaling of the second kind is found to be excellent and scaling of the first kind to be quite good.

At larger energy loss, a broad peak due to quasi-elastic electron-nucleon scattering appears; this peak - very wide due to nuclear Fermi motion - corresponds to processes where the electron scatters from an individual, moving nucleon, which, after interaction with other nucleons, is ejected from the target.
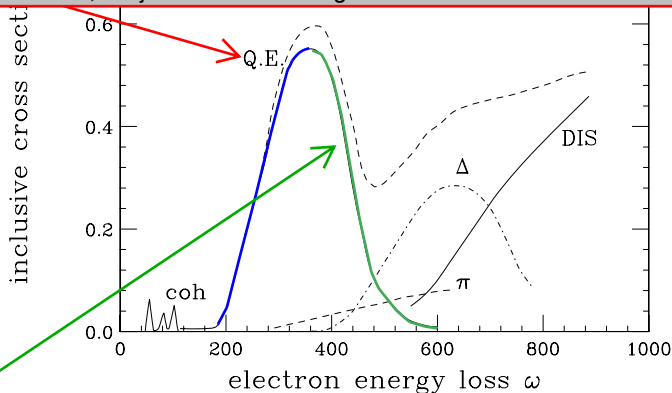
Above the peak scaling of the second kind is good; however, scaling of the first kind is clearly violated. The last occurs for well-understood reasons, namely, in that region one has processes other than quasi-free knockout of nucleons playing an important role.

At very large ω, a structureless continuum due to Deep Inelastic Scattering on quarks bound in nucleons appears.
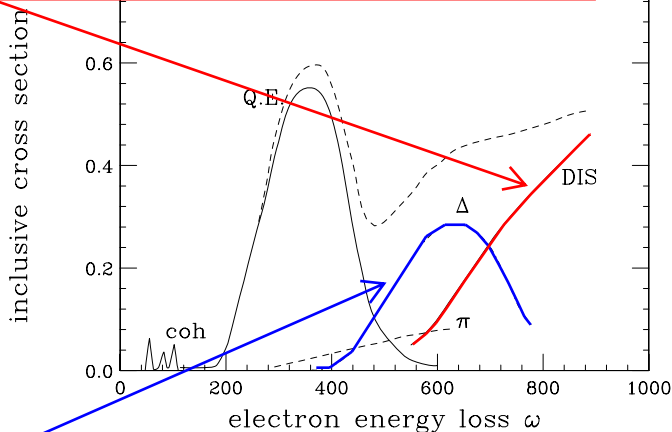
At even larger ω peaks that correspond to excitation of the nucleon to distinct resonances are visible - Δ.

Relativistic Fermi Gas (RFG) (without interaction between the nucleons)

k_F – Fermi momentum

$\eta_F = k_F/m_N$ – dimensionless Fermi momentum

$\xi_F = \sqrt{1 + \eta_F^2} - 1$ – dimensionless Fermi kinetic energy

$$\omega' \equiv \omega - E_{shift},$$

E_{shift} is chosen empirically. It accounts for the effects of both the binding in the initial state and the interaction strength in the final state

$$\lambda' \equiv \omega'/2m_N, \quad \tau' \equiv \kappa^2 - {\lambda'}^2.$$

Dimensionless scaling variable ψ':

$$\psi' = \frac{1}{\sqrt{\xi_F}} \frac{\lambda' - \tau'}{\sqrt{(1 + \lambda')\tau' + \kappa\sqrt{\tau'(1 + \tau')}}}. \tag{1}$$

The physical meaning of ψ'^2 (in units of the Fermi energy) is the smallest kinetic energy that one of the nucleons responding to an external probe can have.

$$F(\kappa, \psi') \equiv \frac{d^2\sigma/d\Omega_e d\omega'}{\sigma_M[v_L G_L(\kappa, \lambda') + v_T G_T(\kappa, \lambda')]} \qquad (2)$$

σ_M – Mott cross section; $d^2\sigma/d\Omega_e d\omega'$ – the cross section of the inclusive electron scattering;

v_L, v_T – Rosenbluth lepton kinematical factors;

G_L, G_T – single-nucleon responses expressed by Sachs form factors, functions of τ', $G_{E_{p,n}}$ and $G_{M_{p,n}}$.

In the Relativistic Fermi Gas model the spectral function:

$$\tilde{S}^{\mathrm{RFG}}(p, \mathcal{E}) = \frac{3A}{8\pi k_F^3} \theta(k_F - p) \delta\left[\mathcal{E}(p) - \mathcal{E}^{\mathrm{RFG}}(p)\right]; \qquad (3)$$

$$\mathcal{E}^{\mathrm{RFG}}(p) = \left(\sqrt{k_F^2 + m_N^2} - \sqrt{p^2 + m_N^2}\right). \qquad (4)$$

$$F(q,y) \overset{q \to \infty}{\longrightarrow} F(y) = 2\pi \int\limits_{-|y|}^{\infty} p\,dp\,\widetilde{n}(y,p), \qquad (5)$$

$$\widetilde{n}(y,p) = \int\limits_{0}^{\mathcal{E}^-} d\mathcal{E}\,\widetilde{S}(p,\mathcal{E}), \qquad (6)$$

$$\lim_{q \to \infty} \mathcal{E}^-(q,y,p) = y + p - \\ - \left(\sqrt{((M_{A-1}^0)^2 + p^2)} - \sqrt{((M_{A-1}^0)^2 + y^2)} \right), \quad (7)$$

$$F_L^{\mathrm{RFG}}(\psi') = \frac{3\xi_F}{2m_N\eta_F^3}(1-\psi'^2)\theta(1-\psi'^2)\left[1+\frac{1}{2}\xi_F(1+\psi'^2)\right]. \quad (8)$$

In the RFG model:

$$F^{\mathrm{RFG}} = F_T^{\mathrm{RFG}} = F_L^{\mathrm{RFG}}. \qquad (9)$$

Dimensionless scaling function:

$$f_{\mathrm{RFG}}(\psi') = k_F \cdot F^{\mathrm{RFG}}(\psi') = \frac{3}{4}(1 - \psi'^2)\Theta(1 - \psi'^2)\frac{1}{\eta_F^2} \times$$
$$\times \left\{ \eta_F^2 + \psi'^2 \left[2 + \eta_F^2 - 2\sqrt{1 + \eta_F^2} \right] \right\} \simeq$$
$$\underset{(\eta_F^2 \ll 1)}{\simeq} \frac{3}{4}(1 - \psi'^2)\Theta(1 - \psi'^2) \tag{10}$$

📄 M. Barbaro *et al.*, *Nucl. Phys. A* **643**, 137 (1998).

The scaling function shows:

- scaling of the first kind: a very weak dependence of $f(\psi')$ on the momentum transfer $q \gtrsim 500$ MeV/c (below the quasielastic peak);

- scaling of the second kind: independence of the mass number A for a wide range of nuclei from ^{4}He to ^{197}Au.

When both types of scaling occur one says that the reduced cross section exhibit superscaling.

📄 T. W. Donnelly and I. Sick, *Phys. Rev. Lett.* **82**, 3212 (1999); *Phys. Rev. C* **60**, 065502 (1999).

However, in RFG $f_{\text{RFG}}^{\text{QE}}(\psi') = 0$ for $\psi' \leq -1$, whereas the experimental scaling function $f^{\text{QE}}(\psi')$ extends to $\psi' \approx -2$ in the data for (e, e') processes.

The scaling function shows:

- scaling of the first kind: a very weak dependence of $f(\psi')$ on the momentum transfer $q \gtrsim 500$ MeV/c (below the quasielastic peak);
- scaling of the second kind: independence of the mass number A for a wide range of nuclei from ^{4}He to ^{197}Au.

When both types of scaling occur one says that the reduced cross section exhibit <u>superscaling</u>.

📄 T. W. Donnelly and I. Sick, *Phys. Rev. Lett.* **82**, 3212 (1999); *Phys. Rev. C* **60**, 065502 (1999).

However, in RFG $f_{\mathrm{RFG}}^{\mathrm{QE}}(\psi') = 0$ for $\psi' \leq -1$, whereas the experimental scaling function $f^{\mathrm{QE}}(\psi')$ extends to $\psi' \approx -2$ in the data for (e, e') processes.

The scaling function shows:

- scaling of the first kind: a very weak dependence of $f(\psi')$ on the momentum transfer $q \gtrsim 500$ MeV/c (below the quasielastic peak);

- scaling of the second kind: independence of the mass number A for a wide range of nuclei from ^{4}He to ^{197}Au.

When both types of scaling occur one says that the reduced cross section exhibit <u>superscaling</u>.

📄 T. W. Donnelly and I. Sick, *Phys. Rev. Lett.* **82**, 3212 (1999); *Phys. Rev. C* **60**, 065502 (1999).

However, in RFG $f^{\mathrm{QE}}_{\mathrm{RFG}}(\psi') = 0$ for $\psi' \leq -1$, whereas the experimental scaling function $f^{\mathrm{QE}}(\psi')$ extends to $\psi' \approx -2$ in the data for (e, e') processes.

Thus, it became necessary to consider the superscaling in theoretical methods which go beyond the RFG. One of them is the Coherent Density Fluctuation Model (CDFM) that is a natural extension of the Fermi gas case to realistic finite nuclear system beyond the mean field approximation. The accounting for NN correlations in CDFM in the momentum and density distribution made it possible to reproduce the available experimental data for $\psi' < 0$, including $\psi' \lesssim -1$.

📄 A. N. Antonov, V. A. Nikolaev, and I. Zh. Petkov, *Bulg. J. Phys.* **6**, 151 (1979); *Z. Phys. A* **297**, 257 (1980); *ibid.* **304**, 239 (1982); *Nuovo Cimento A* **86**, 23 (1985).

📄 A. N. Antonov, P. E. Hodgson, and I. Zh. Petkov, *Nucleon Momentum and Density Distributions in Nuclei* (Clarendon Press, Oxford, 1988); *Nucleon Correlations in Nuclei* (Springer-Verlag, Berlin-Heidelberg-New York, 1993).
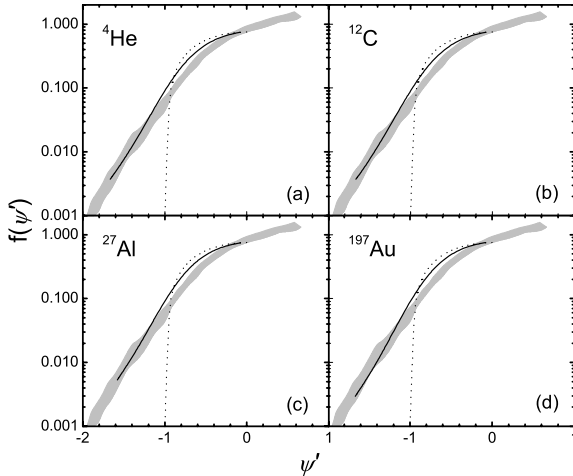
Figure: Scaling function $f(\psi')$ in the CDFM (solid line) at $q = 1560$ MeV/c for ^{4}He, ^{12}C, ^{27}Al, and ^{197}Au. The experimental data are given by the shaded area. The RFG result is shown by dotted line.

SUPERSCALING & CDFM

A. N. Antonov et al., "Superscaling in nuclei: A search for a scaling function beyond the relativistic Fermi gas model", *Phys. Rev. C* **69**, 044321 (2004).

A. N. Antonov et al., "Superscaling , scaling functions, and nucleon momentum distributions in nuclei", *Phys. Rev. C* **71**, 014317 (2005).

A. N. Antonov et al., "Scaling functions and superscaling in medium and heavy nuclei", *Phys. Rev. C* **73**, 047302 (2006).

A. N. Antonov et al., "Superscaling analysis of inclusive electron scattering and its extension to charge-changing neutrino-nucleus cross sections beyond the relativistic Fermi gas approach", *Phys. Rev. C* **74**, 054603 (2006).

A. N. Antonov et al., "Superscaling in a dilute Fermi gas and the nucleon momentum distribution in nuclei", *Phys. Rev. C* **75**, 034319 (2007).

A. N. Antonov et al., "Superscaling and neutral current quasielastic neutrino-nucleus scattering beyond the relativistic Fermi gas model", *Phys. Rev. C* **75**, 064617 (2007).

M. V. Ivanov et al., "Superscaling and charge-changing neutrino scattering from nuclei in the Δ region beyond the relativistic Fermi gas model", *Phys. Rev. C* **77**, 034612 (2008).

Aims of the present work:

I To consider the NN forces in the nuclear medium and their effect on the components of the nucleon momentum distribution in relation to the superscaling analysis. To study the role of $n(k)$ on the behavior of the quasielastic (QE) scaling function.

II To extend the superscaling analysis of the QE electron scattering to predict charge-changing (CC) neutrino-nucleus scattering cross sections in the QE and Δ-region.

III To extend the superscaling analysis for calculations of QE scattering via the weak neutral current (NC) of neutrinos and antineutrinos from nuclei.

For this purpose for point **I**:

1. We use firstly the momentum distribution in a hard-sphere dilute Fermi gas model (HSDFG) to calculate the scaling function.

2. We attempt to throw light on the connection between the generally established high-momentum asymptotics of $n(k)$ and the QE scaling function. This makes it possible to establish (at least approximately) the particular form of the power-law decrease of $n(k)$ at large values of k and thus, to extract additional information about the NN forces from the description of the superscaling phenomenon.

The hard-sphere dilute Fermi gas (HSDFG) is a low density gas of fermions that interact via a repulsive hard-core potential.

📄 A. B. Migdal, *Zh. Eksp. Teor. Fiz.* **32**, 333 (1957); [*Sov. Phys. JETP* **5**, 333 (1957)];

📄 V. M. Galitskii, *Zh. Eksp. Teor. Fiz.* **34**, 151 (1958); [*Sov. Phys. JETP* **7**, 104 (1958)];

📄 V. A. Belyakov, *Zh. Eksp. Teor. Fiz.* **40**, 1210 (1961); [*Sov. Phys. JETP* **13**, 850 (1961)];

📄 W. Czyż and K. Gottfried, *Nucl. Phys.* **21**, 676 (1961);

📄 R. Sartor and C. Mahaux, *Phys. Rev. C* **21**, 1546 (1980); *Phys. Rev. C* **25**, 677 (1982).

In the HSDFG: parameter $k_F c$, where c denotes the hard-core radius of NN interactions or it is identified with the scattering length in free space , k_F is the Fermi momentum. Usually: $k_F c = 0.70$ ($c = 0.50$ fm, $k_F = 1.40$ fm^{-1}). As shown by Migdal $n(k)$ in the normal Fermi gas is discontinuous at the Fermi momentum $k = k_F$. This discontinuity is an inherent consequence of an arbitrary interaction between particles in an infinite system. In the HSDFG:

$$n(k) = n_<(k) + n_>(k) \text{ with } \begin{cases} n_<(k) = 0 \text{ for } k > k_F \\ n_>(k) = 0 \text{ for } k < k_F \end{cases} . \qquad (1)$$
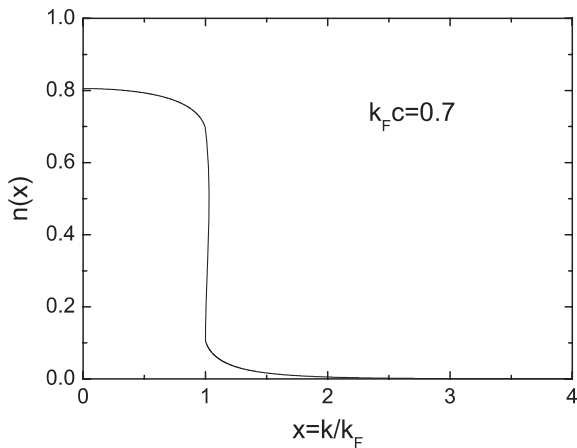
Figure: The momentum distribution $n(k)$ in hard-sphere dilute Fermi gas as a function of $x = k/k_F$.

At $k < k_F$:

$$n_<(k) = 1 - \frac{\nu-1}{3\pi^2 x}(k_F c)^2 \left[(7\ln 2 - 8)x^3 + (10 - 3\ln 2)x + \right.$$
$$\left. + 2\ln\frac{1+x}{1-x} - 2(2-x^2)^{3/2}\ln\frac{(2-x^2)^{1/2}+x}{(2-x^2)^{1/2}-x} \right], \qquad (2)$$

where $x = k/k_F$ and $\nu = 4$ is adopted.
At $1 < x < \sqrt{2}$:

$$n_>(k) = \frac{\nu-1}{6\pi^2 x}(k_F c)^2 \left\{ (7x^3 - 3x - 6)\ln\frac{x-1}{x+1} + \right.$$
$$+ (7x^3 - 3x + 2)\ln 2 - 8x^3 + 22x^2 + 6x - 24 +$$
$$+ 2(2-x^2)^{3/2} \left\{ \ln\frac{2+x+(2-x^2)^{1/2}}{2+x-(2-x^2)^{1/2}} + \right.$$
$$\left. \left. + \ln\frac{1+(2-x^2)^{1/2}}{1-(2-x^2)^{1/2}} - 2\ln\frac{x+(2-x^2)^{1/2}}{x-(2-x^2)^{1/2}} \right\} \right\}. \qquad (3)$$

At $\sqrt{2} < x < 3$:

$$n_>(k) = \frac{\nu - 1}{6\pi^2 x}(k_F c)^2 \left\{ (7x^3 - 3x - 6) \ln \frac{x-1}{x+1} - 8x^3 + 22x^2 + \right.$$
$$+ 6x - 24 + (7x^3 - 3x + 2) \ln 2 - 4(x^2 - 2)^{3/2} \times$$
$$\times \left\{ \arctan \frac{(x+2)}{(x^2-2)^{1/2}} + \arctan \frac{1}{(x^2-2)^{1/2}} - \right.$$
$$\left. \left. - 2 \arctan \frac{x}{(x^2-2)^{1/2}} \right\} \right\}. \tag{4}$$

At $x > 3$:

$$n_>(k) = 2\frac{\nu - 1}{3\pi^2 x}(k_F c)^2 \left\{ 2 \ln \frac{x+1}{x-1} - 2x + (x^2 - 2)^{3/2} \times \right.$$
$$\times \left\{ 2 \arctan \frac{x}{(x^2-2)^{1/2}} - \arctan \frac{x-2}{(x^2-2)^{1/2}} - \right.$$
$$\left. \left. - \arctan \frac{(x+2)}{(x^2-2)^{1/2}} \right\} \right\}. \tag{5}$$

$$f^{\text{HSDFG}}(\psi') = \frac{3}{2} \int\limits_{|\zeta|/\eta_F}^{\infty} xn(x)dx, \qquad (6)$$

$\eta_F = k_F/m_N$

$$\zeta = \psi'\left\{\left[\sqrt{1+\eta_F^2}-1\right]\left[2+\psi'^2\left(\sqrt{1+\eta_F^2}-1\right)\right]\right\}^{1/2}. \qquad (7)$$

Since $\eta_F^2 \ll 1$:

$$f^{\text{HSDFG}}(\psi') \simeq \frac{3}{2} \int\limits_{|\psi'|}^{\infty} xn(x)dx. \qquad (8)$$

It follows from Eq. (8) that the HSDFG system also exhibits superscaling.
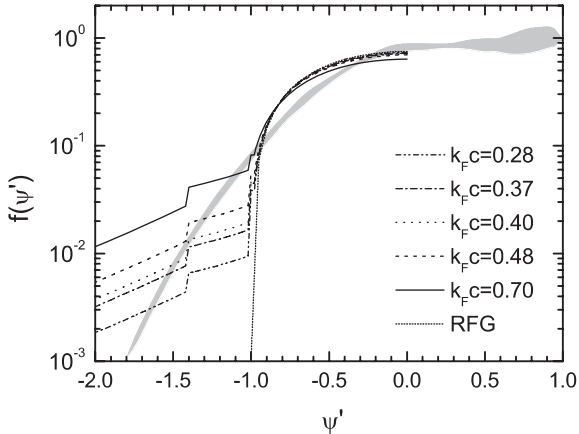
Figure: The scaling function $f(\psi')$ in HSDFG calculated for different values of $k_F c$ in comparison with the RFG model result. The grey area shows experimental data.
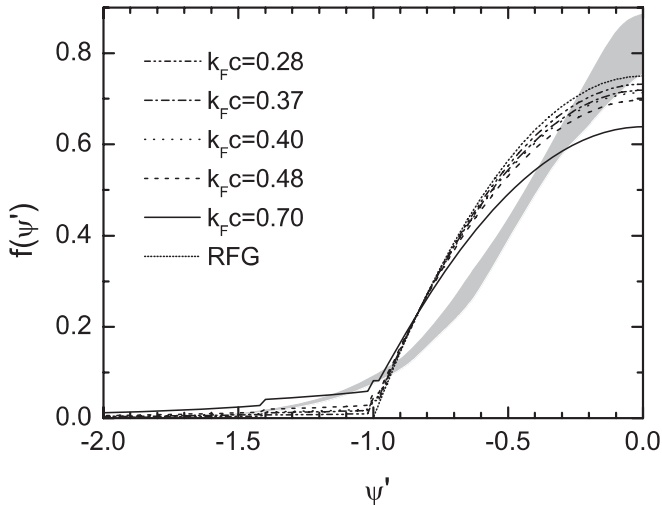
Figure: The same as in previous Figure but in linear scale.

The scaling function is extended for large negative values of ψ' in contrast to the case of the RFG scaling function but the agreement with the experimental data is poor. The step behavior of the scaling function reflects the discontinuity of $n(k)$ at $k = k_F$.

General consideration of the asymptotic behavior of $n(k)$ in:

📄 R. D. Amado and R. M. Woloshyn, *Phys. Lett. B* **62**, 253 (1976);

📄 R. D. Amado, *Phys. Rev. C* **14**, 1264 (1976);

📄 R. D. Amado and R. M. Woloshyn, *Phys. Rev. C* **15**, 2200 (1977).

At large k, $n(k)$ has a power-low decrease

$$n(k) \xrightarrow[k\to\infty]{} \left[\frac{\widetilde{V}_{NN}(k)}{k^2} \right]^2. \qquad (1)$$

$\widetilde{V}_{NN}(k)$ is the Fourier transform of the NN interaction $V_{NN}(r)$.
For δ-forces (as in the HSDFG):

$$n(k) \sim 1/k^4$$

Under question: k or k/A must be large for Eq. (1) to apply?
Typically $n(k) \sim 1/k^{4+m}$, $m > 0$ (i.e. $\widetilde{V}_{NN}(k) \sim \dfrac{1}{k^{m/2}}$).
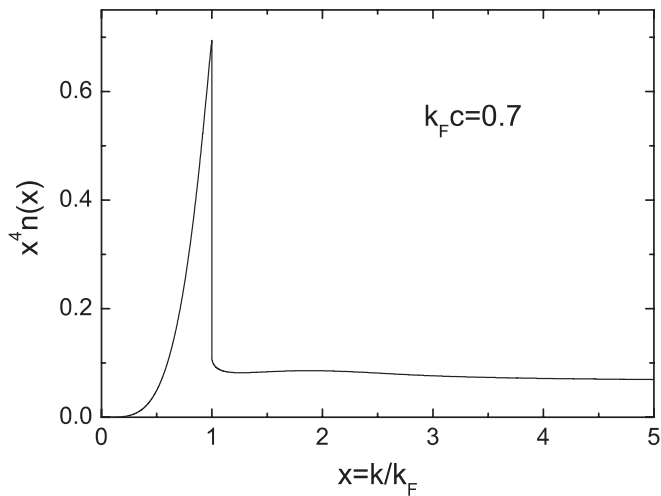
Figure: The momentum distribution in HSDFG $n(x)$ multiplied by $x^4 = (k/k_F)^4$.

It can be seen that $n(k)$ in the HSDFG decreases like $\sim 1/k^{4+m}$ with a small value of m.

Next: we study the question about the general feature of $\widetilde{V}_{NN}(k)$ that results in $n(k)$ with a power-law behavior that best agrees with the scaling function.

We assume $V_{NN}(r)$ different from a δ-function and calculate the scaling function $f(\psi')$ using different asymptotics for $n(k)$ in the dilute Fermi gas at $k > k_F$. We look for the proper value of m. For $k < k_F$ we use $n(k)$ [Eq. (2) from HSDFG]. For $k > k_F$ ($k_F c = 0.70$):

$$n(k) = N\frac{1}{k^{4+m}}, \tag{2}$$

$$N = \frac{0.24}{3}(1+m)k_F^{4+m}. \tag{3}$$

The total normalization is:

$$\frac{3}{4\pi k_F^3} \int n(\vec{k}) d^3 \vec{k} = 1. \tag{4}$$

Finally

$$f(\psi') = 0.12 \left(\frac{1+m}{2+m} \right) \frac{1}{|\psi'|^{2+m}}. \tag{5}$$
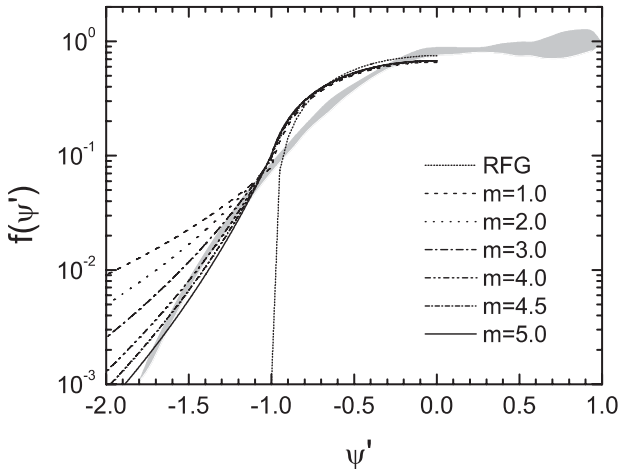
Figure: The scaling function in a dilute Fermi gas for different values of m in the asymptotics of the momentum distribution $n(k) \sim 1/k^{4+m}$ given in comparison with the RFG result. The grey area shows experimental data.

Agreement with the experimental QE scaling function is achieved when $\boxed{m \approx 4.5}$ in Eqs. (2), (3) and (5), *i.e.*

$$n(k) \approx \frac{1}{k^{8.5}}. \qquad (6)$$

In CDFM:

$$n(k) \sim \frac{1}{k^8}, \qquad (7)$$

i.e. $n(k) \sim 1/k^{4+m}$ with $\boxed{m = 4}$.
The inverse Fourier transform gives

$$V_{NN}(r) \sim \frac{1}{r} \text{ for } m = 4; \qquad V_{NN}(r) \sim \frac{1}{r^{1/2}} \text{ for } m = 5.$$

The behavior of the QE scaling function depends mainly on the particular form of the power-law asymptotics of $n(k)$.

Conclusions from point I:

i) The superscaling considered within the model of dilute Fermi gas with interactions between particles gives an improvement over the results of the relativistic noninteracting Fermi gas model, allowing one to describe the QE scaling function for $\psi' < -1$, whereas the RFG model gives $f(\psi') = 0$ in this region.

ii) It is established that the hard-sphere (with delta-forces between nucleons) approximation for the dilute Fermi gas is quite a rough one. The use of more realistic NN forces leading to $m \simeq 4.5$ instead of $m = 0$ (for delta-force) in the well-known power-law asymptotics of the momentum distribution $n(k) \sim 1/k^{4+m}$ at large k leads to a good explanation of the data for the ψ'-scaling function in inclusive electron scattering from a wide range of nuclei.

Conclusions from point **I**:

i) The superscaling considered within the model of dilute Fermi gas with interactions between particles gives an improvement over the results of the relativistic noninteracting Fermi gas model, allowing one to describe the QE scaling function for $\psi' < -1$, whereas the RFG model gives $f(\psi') = 0$ in this region.

ii) It is established that the hard-sphere (with delta-forces between nucleons) approximation for the dilute Fermi gas is quite a rough one. The use of more realistic NN forces leading to $m \simeq 4.5$ instead of $m = 0$ (for delta-force) in the well-known power-law asymptotics of the momentum distribution $n(k) \sim 1/k^{4+m}$ at large k leads to a good explanation of the data for the ψ'-scaling function in inclusive electron scattering from a wide range of nuclei.

iii) The asymptotics of $n(k) \sim 1/k^{8.5}$ found in the dilute Fermi gas by optimal fit to the data for $f(\psi')$ is similar to that in the CDFM ($\sim 1/k^8$) which, being a theoretical correlation model, describes the superscaling in the quasielastic part of the electron-nucleus scattering. Thus, the momentum distribution in the dilute Fermi-gas model with realistic NN forces can serve as an "effective" momentum distribution (a step-like one with a discontinuity) which gives a similar result for $f(\psi')$ as the correlation methods for realistic finite nuclear systems. It can be concluded that the momentum distribution with asymptotics from $\sim 1/k^8$ to $\sim 1/k^{8.5}$ is the proper one for explaining the phenomenological shape of the scaling function obtained from inclusive QE electron scattering.

The superscaling is due to the *specific high-momentum tail* of $n(k)$ similar for all nuclei which is known to be caused by the short-range and tensor correlations related *to peculiarities of the NN forces* near their core.

The main result of the present work might be the observation that the values of $f(\psi')$ for $\psi' < -1$ depend on *the particular form* of the power-law asymptotics of $n(k)$ at large k which is related to *a corresponding particular behavior* of the *in-medium NN forces* around the core.

We point out that the power-law decrease of $n(k)$ as $\sim 1/k^{4+m}$ with $m \simeq 4.5$ in the interacting dilute Fermi gas is the proper one and it is close to that obtained in CDFM ($m = 4$) which describes the superscaling correctly as well.

The superscaling is due to the *specific high-momentum tail* of $n(k)$ similar for all nuclei which is known to be caused by the short-range and tensor correlations related *to peculiarities of the NN forces* near their core.

The main result of the present work might be the observation that the values of $f(\psi')$ for $\psi' < -1$ depend on *the particular form* of the power-law asymptotics of $n(k)$ at large k which is related to *a corresponding particular behavior* of the *in-medium NN forces* around the core.

We point out that the power-law decrease of $n(k)$ as $\sim 1/k^{4+m}$ with $m \simeq 4.5$ in the interacting dilute Fermi gas is the proper one and it is close to that obtained in CDFM ($m = 4$) which describes the superscaling correctly as well.

The superscaling is due to the *specific high-momentum tail* of $n(k)$ similar for all nuclei which is known to be caused by the short-range and tensor correlations related *to peculiarities of the NN forces* near their core.

The main result of the present work might be the observation that the values of $f(\psi')$ for $\psi' < -1$ depend on *the particular form* of the power-law asymptotics of $n(k)$ at large k which is related to *a corresponding particular behavior* of the *in-medium NN forces* around the core.

We point out that the power-law decrease of $n(k)$ as $\sim 1/k^{4+m}$ with $m \simeq 4.5$ in the interacting dilute Fermi gas is the proper one and it is close to that obtained in CDFM ($m = 4$) which describes the superscaling correctly as well.

The NN force for $m = 4$ is expected to go as $V_{NN}(r) \sim 1/r$ and for $m = 5$ to go as $V_{NN}(r) \sim (1/r)^{1/2}$.

The conclusion is that the important property of the repulsive short-range core (leading to NN correlations and high-momentum tail of $n(k)$) is that it goes to infinity for $r \to 0$ as $1/r$ or softer.

The link between the asymptotic behavior of $n(k)$ and NN force implies that inclusive QE electron scattering from nuclei provides important information on the NN forces in the nuclear medium.

The NN force for $m = 4$ is expected to go as $V_{NN}(r) \sim 1/r$ and for $m = 5$ to go as $V_{NN}(r) \sim (1/r)^{1/2}$.

The conclusion is that the important property of the repulsive short-range core (leading to NN correlations and high-momentum tail of $n(k)$) is that it goes to infinity for $r \to 0$ as $1/r$ or softer.

The link between the asymptotic behavior of $n(k)$ and NN force implies that inclusive QE electron scattering from nuclei provides important information on the NN forces in the nuclear medium.

The NN force for $m = 4$ is expected to go as $V_{NN}(r) \sim 1/r$ and for $m = 5$ to go as $V_{NN}(r) \sim (1/r)^{1/2}$.

The conclusion is that the important property of the repulsive short-range core (leading to NN correlations and high-momentum tail of $n(k)$) is that it goes to infinity for $r \to 0$ as $1/r$ or softer.

The link between the asymptotic behavior of $n(k)$ and NN force implies that inclusive QE electron scattering from nuclei provides important information on the NN forces in the nuclear medium.

A.N. Antonov, M.V. Ivanov, M.K. Gaidarov, E. Moya de Guerra, "Superscaling in a dilute Fermi gas and the nucleon momentum distribution in nuclei", *Phys. Rev. C* **75**, 034319 (2007).

4.1 Basic Relationship of the Coherent Density Fluctuation Model

Generator Coordinate Method Equations

$$\Psi(\mathbf{r}_1, ..., \mathbf{r}_A) = \int F(x_1, x_2, ...)\Phi(\mathbf{r}_1, ..., \mathbf{r}_A; x_1, x_2, ...)dx_1 dx_2... \quad (1)$$

– The Hill-Wheeler equation

$$\int [\mathcal{H}(x, x') - E\mathcal{I}(x, x')]F(x')dx' = 0 \quad (2)$$

– The overlap and energy kernels

$$\mathcal{I}(x, x') = \langle \Phi(\{\mathbf{r}_i\}, x) | \Phi(\{\mathbf{r}_i\}, x') \rangle \quad (3)$$

$$\mathcal{H}(x, x') = \langle \Phi(\{\mathbf{r}_i\}, x) | \hat{H} | \Phi(\{\mathbf{r}_i\}, x') \rangle \quad (4)$$

– For many-fermion systems the kernels $\mathcal{I}(x, x')$ and $\mathcal{H}(x, x')$ peak strongly at $x \sim x'$

$$\mathcal{I}(x, x') \simeq \mathcal{I}(x, x)\mathcal{G}(x - x') \quad (5)$$

$$\mathcal{H}(x, x') \simeq \mathcal{H}(x, x)\mathcal{G}(x - x') \quad (6)$$

Coherent Density Fluctuation Model

– Delta-function approximation

$$\mathcal{I}(x, x') \to \delta(x - x') \tag{7}$$

$$\mathcal{H}(x, x') \to -\frac{\hbar^2}{2m_{eff}}\delta''(x - x') + V\left(\frac{x + x'}{2}\right)\delta(x - x') \tag{8}$$

and the weight function is determined under the condition

$$\int\limits_0^\infty |F(x)|^2 dx = 1 \tag{9}$$

leads to the relationships:

$$\int \Phi^*(\mathbf{r}, \mathbf{r}_2, ..., \mathbf{r}_A, x')\Phi(\mathbf{r}', \mathbf{r}_2, ..., \mathbf{r}_A, x)d\mathbf{r}_2...d\mathbf{r}_A \cong \rho_{x,x}(\mathbf{r}, \mathbf{r}')\delta(x - x') \tag{10}$$

$$\rho_{x,x}(\mathbf{r}, \mathbf{r}') \equiv \rho_x(\mathbf{r}, \mathbf{r}') =$$
$$= \frac{A}{\langle \Phi | \Phi \rangle_x} \int \Phi^*(\mathbf{r}, \mathbf{r}_2, ..., \mathbf{r}_A, x) \Phi(\mathbf{r}', \mathbf{r}_2, ..., \mathbf{r}_A, x) d\mathbf{r}_2...d\mathbf{r}_A, \quad (11)$$

where

$$\langle \Phi | \Phi \rangle_x \equiv \int \Phi^*(\mathbf{r}_1, ..., \mathbf{r}_A, x) \Phi(\mathbf{r}_1, ..., \mathbf{r}_A, x) d\mathbf{r}_1...d\mathbf{r}_A; \quad (12)$$

– In the CDFM the generating function $\Phi(\{\mathbf{r}_i\}, x)$ describes a system corresponding to a piece of nuclear matter with a one-body density matrix

$$\rho_x(\mathbf{r}, \mathbf{r}') = 3\rho_0(x) \frac{j_1(k_F(x)|\mathbf{r} - \mathbf{r}'|)}{(k_F(x)|\mathbf{r} - \mathbf{r}'|)} \Theta\left(x - \frac{|\mathbf{r} + \mathbf{r}'|}{2}\right) \quad (13)$$

and uniform density

$$\rho_x(\mathbf{r}) = \rho_0(x)\Theta(x - |\mathbf{r}|), \tag{14}$$

where

$$\rho_0(x) = \frac{3A}{4\pi x^3} \tag{15}$$

and the generator coordinate x is the radius of a sphere containing all A nucleons in it.

$$k_F(x) = \left(\frac{3\pi^2}{2}\rho_0(x)\right)^{1/3} \equiv \frac{\alpha}{x} \quad \text{with} \quad \alpha = \left(\frac{9\pi A}{8}\right)^{1/3} \simeq 1.52A^{1/3} \tag{16}$$

is the Fermi momentum of such a piece of nuclear matter.
One-body density matrix (ODM) of the system in the CDFM

$$\rho(\mathbf{r}, \mathbf{r}') = \int\limits_0^\infty dx |F(x)|^2 \rho_x(\mathbf{r}, \mathbf{r}') \tag{17}$$

The Wigner distribution function which corresponds to the ODM

$$W(\mathbf{r}, \mathbf{k}) = \frac{4}{(2\pi)^3} \int\limits_0^\infty dx |F(x)|^2 \Theta(x - |\mathbf{r}|)\Theta(k_F(x) - |\mathbf{k}|) \quad (18)$$

$$\rho(\mathbf{r}) = \int d\mathbf{k} W(\mathbf{r}, \mathbf{k}) = \int\limits_0^\infty dx |F(x)|^2 \frac{3A}{4\pi x^3} \Theta(x - |\mathbf{r}|), \quad (19)$$

$$n(\mathbf{k}) = \int d\mathbf{r} W(\mathbf{r}, \mathbf{k}) = \frac{4}{(2\pi)^3} \int_0^\infty dx |F(x)|^2 \frac{4\pi x^3}{3} \Theta(k_F(x) - |\mathbf{k}|)$$
$$= \frac{4}{(2\pi)^3} \int_0^{\alpha/k} dx |F(x)|^2 \frac{4}{3}\pi x^3 \quad (20)$$

$$|\mathcal{F}(x)|^2 = -\frac{1}{\rho_0(x)} \left.\frac{d\rho(r)}{dr}\right|_{r=x} \quad \text{at} \quad \frac{d\rho(r)}{dr} \leq 0 \qquad (21)$$

$$|\mathcal{F}(x)|^2 = -\frac{3\pi^2}{2}\frac{\alpha}{x^5} \left.\frac{dn(k)}{dk}\right|_{k=\frac{\alpha}{x}} \quad \text{at} \quad \frac{dn(k)}{dk} \leq 0 \qquad (22)$$

$$\int \rho(\mathbf{r})d\mathbf{r} = A; \quad \int n(\mathbf{k})d\mathbf{k} = A \qquad (23)$$

$$\int\limits_0^\infty |F(x)|^2 dx = 1 \qquad (24)$$

Our basic assumption within the CDFM is that the scaling function for a finite nucleus $f(\psi')$ can be defined by means of the weight function $|F(x)|$, weighting the scaling function for the RFG at given x.

$$f(\psi') = \int\limits_0^{\alpha/(k_F|\psi'|)} dx |F(x)|^2 \frac{3}{4} \left[1 - \left(\frac{k_F x \psi'}{\alpha} \right)^2 \right] \times$$

$$\times \left\{ 1 + \left(\frac{x m_N}{\alpha} \right)^2 \left(\frac{k_F x \psi'}{\alpha} \right)^2 \left[2 + \left(\frac{\alpha}{x m_N} \right)^2 - 2 \sqrt{1 + \left(\frac{\alpha}{x m_N} \right)^2} \right] \right\}$$

$$(25)$$

$$f(\psi') = \int\limits_{0}^{\alpha/(k_F|\psi'|)} |\mathcal{F}(x)|^2 f(\psi', x) dx \qquad (26)$$

$$|\mathcal{F}(x)|^2 = -\frac{1}{\rho_0(x)} \left.\frac{d\rho(r)}{dr}\right|_{r=x}, \ \rho_0(x) = \frac{3A}{4\pi x^3}, \ \alpha = \left(\frac{9\pi A}{8}\right)^{1/3} \qquad (27)$$

$$f(\psi') = \frac{4\pi}{A} \int\limits_{0}^{\alpha/(k_F|\psi'|)} \rho(x) \left[x^2 f(\psi', x) + \frac{x^3}{3} \frac{df(\psi', x)}{dx}\right] dx \qquad (28)$$

$$f(\psi', x) = \frac{3}{4}\left[1 - \left(\frac{k_F x \psi'}{\alpha}\right)^2\right] \left\{1 + \left(\frac{x m_N}{\alpha}\right)^2 \left(\frac{k_F x \psi'}{\alpha}\right)^2 \times \right.$$
$$\left. \times \left[2 + \left(\frac{\alpha}{x m_N}\right)^2 - 2\sqrt{1 + \left(\frac{\alpha}{x m_N}\right)^2}\right]\right\} \qquad (29)$$

$$|F(x)|^2 = -\frac{3\pi^2}{2}\frac{\alpha}{x^5}\left.\frac{dn(k)}{dk}\right|_{k=\frac{\alpha}{x}} \tag{30}$$

$$f(\psi') = \frac{4\pi}{A}\int\limits_{k_F|\psi'|}^{\infty} n(k)\left[k^2 f(\psi',k) + \frac{k^3}{3}\frac{df(\psi',k)}{dk}\right]dk \tag{31}$$

$$\lim_{k\to\infty} n(k)k^3 = 0 \tag{32}$$

$$f(\psi',k) = \frac{3}{4}\left[1 - \left(\frac{k_F\psi'}{k}\right)^2\right]\left\{1 + \left(\frac{m_N}{k}\right)^2\left(\frac{k_F\psi'}{k}\right)^2 \times\right.$$
$$\left.\times\left[2 + \left(\frac{k}{m_N}\right)^2 - 2\sqrt{1 + \left(\frac{k}{m_N}\right)^2}\right]\right\} \tag{33}$$

4.2 CDFM$_I$ Scaling Functions in the QE Region

The total scaling function is expressed by the sum of the proton $f_p^{QE}(\psi')$ and neutron $f_n^{QE}(\psi')$ scaling functions, which are determined by the proton and neutron densities $\rho_p(r)$ and $\rho_n(r)$ (or by corresponding momentum distributions), respectively:

$$f^{QE}(\psi') = \frac{1}{A}[Zf_p^{QE}(\psi') + Nf_n^{QE}(\psi')]. \tag{34}$$

$f_p^{QE}(\psi')$ and $f_n^{QE}(\psi')$ scaling functions can to present as sums of scaling functions for negative ($f_{p(n),1}^{QE}(\psi')$) and positive ($f_{p(n),2}^{QE}(\psi')$) values of ψ':

$$f_{p(n)}^{QE}(\psi') = f_{p(n),1}^{QE}(\psi') + f_{p(n),2}^{QE}(\psi'). \tag{35}$$

We include a parameter c_1 which gives correct maximum value and also an asymmetric tail in $f^{QE}(\psi')$ for $\psi' \geq 0$.

$$f_{p(n),1}^{\mathrm{QE}}(\psi') = \int\limits_{0}^{\alpha_{p(n)}/(k_F^{p(n)}|\psi'|)} dR |F_{p(n)}(R)|^2 f_{\mathrm{RFG},1}^{p(n)}(\psi'(R)), \ \psi' \leq 0, \quad (36)$$

$$f_{p(n),2}^{\mathrm{QE}}(\psi') = \int\limits_{0}^{c_2\alpha_{p(n)}/(k_F^{p(n)}\psi')} dR |F_{p(n)}(R)|^2 f_{\mathrm{RFG},2}^{p(n)}(\psi'(R)), \ \psi' \geq 0, \quad (37)$$

where

$$f_{\mathrm{RFG},1}^{p(n)}(\psi'(R)) = c_1 \left[1 - \left(\frac{k_F^{p(n)} R |\psi'|}{\alpha_{p(n)}} \right)^2 \right], \ \psi' \leq 0 \quad (38)$$

and a exponential form of $f_{\mathrm{RFG},2}^{p(n)}(\psi'(R))$

$$f_{\mathrm{RFG},2}^{p(n)}(\psi'(R)) = c_1 \exp\left[-\frac{k_F^{p(n)} R \psi'}{c_2 \alpha_{p(n)}} \right], \ \psi' \geq 0. \quad (39)$$

or a parabolic form of $f_{\text{RFG},2}^{p(n)}(\psi'(R))$

$$f_{\text{RFG},2}^{p(n)}(\psi'(R)) = c_1 \left[1 - \left(\frac{k_F^{p(n)} R \psi'}{c_2 \alpha_{p(n)}} \right)^2 \right], \ \psi' \geq 0. \qquad (40)$$

The proton and neutron weight functions are obtained from the corresponding proton and neutron densities

$$\left| F_{p(n)}(R) \right|^2 = -\frac{4\pi R^3}{3Z(N)} \left. \frac{d\rho_{p(n)}(r)}{dr} \right|_{r=R}, \qquad (41)$$

$$\alpha_{p(n)} = \left[\frac{9\pi Z(N)}{4} \right]^{1/3}, \qquad (42)$$

$$\int\limits_0^\infty \rho_{p(n)}(\mathbf{r})d\mathbf{r} = Z(N) \qquad (43)$$

Fermi-momentum for the protons and neutrons can be calculated using the expression

$$k_F^{p(n)} = \alpha_{p(n)} \int\limits_0^\infty dR \frac{1}{R} |F_{p(n)}(R)|^2. \tag{44}$$

The functions are normalized as follows:

$$\int\limits_0^\infty |F_{p(n)}(R)|^2 dR = 1, \quad \int\limits_{-\infty}^\infty f_{p(n)}^{\mathrm{QE}}(\psi')d\psi' = 1. \tag{45}$$

$\Rightarrow$

$$\int\limits_{-\infty}^\infty f^{\mathrm{QE}}(\psi')d\psi' = 1 \tag{46}$$

$$c_2 = \frac{3}{2c_1} - 1 \qquad \text{in the case of Eq. (40)}$$

$$c_2 = \frac{1 - (2/3)c_1}{0.632c_1} \qquad \text{in the case of Eq. (39)}$$

It was shown in the case of the electron scattering that the results obtained when asymmetric scaling function $f^{QE}(\psi')$ ($c_1^{QE} = 0.63$) with $f_{RFG,2}^{p(n)}(\psi'(R))$ from Eq. (6) is used agree with the data in cases when the transferred momentum in the position of the maximum of the QE peak extracted from data is $q_{exp}^{QE} < 450$ MeV/c $\approx 2k_F$ and underestimate them when $q_{exp}^{QE} \geq 450$ MeV/c in the region close to the QE peak. In the case of almost symmetric scaling function $f^{QE}(\psi')$ ($c_1^{QE} = 0.72$) the results agree with the data in the region of the QE peak in cases when $q_{exp}^{QE} \geq 450$ MeV/c $\approx 2k_F$ and overestimate them when $q_{exp}^{QE} < 450$ MeV/c.
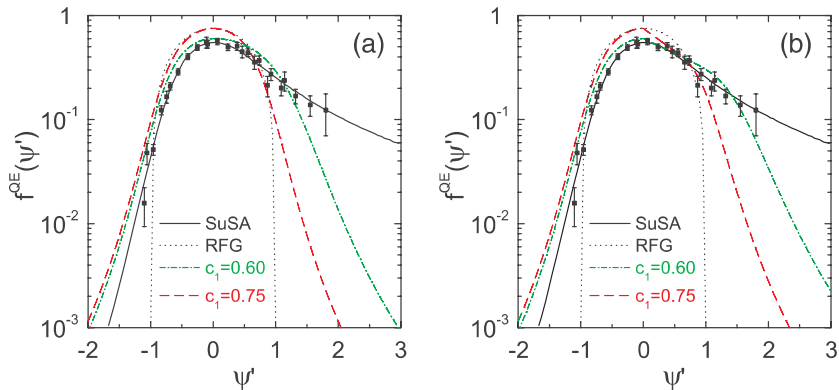
Figure: The quasielastic scaling function $f^{QE}(\psi')$ for ^{12}C calculated in the CDFM using parabolic form (a) and exponential form (b).
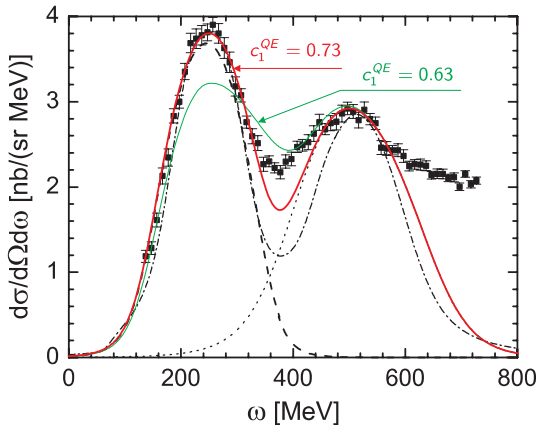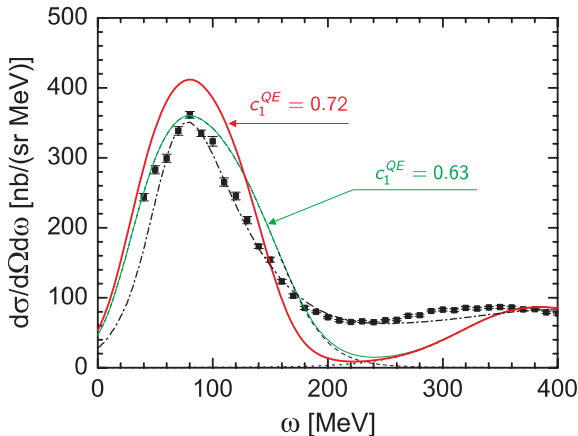
Figure: Inclusive electron scattering on ^{12}C at $\epsilon = 1108$ MeV and $\theta = 37.5°$ ($q_{exp}^{QE} = 675$ MeV/c $> 2k_F$). The results obtained using $c_1^{QE} = 0.73$ in the CDFM scaling function for the QE cross section and the total result are given by dashed and red solid line, respectively. Dotted line: using CDFM Δ-scaling function. Thin green line: total CDFM result with $c_1^{QE} = 0.63$. Dot-dashed line: using QE- and Δ-scaling functions obtained in the LFD approach.

Figure: Inclusive electron scattering on ^{12}C at $\epsilon = 1500$ MeV and $\theta = 13.5°$ ($q_{exp}^{QE} = 352$ MeV/c $\leq 2k_F$). The results obtained using $c_1^{QE} = 0.72$ in the CDFM scaling function for the QE cross section and the total result are given by dashed and red solid line, respectively. Dotted line: using CDFM Δ-scaling function; green solid line: total CDFM result with $c_1^{QE} = 0.63$. Dash-dotted line: result of ERFG method.
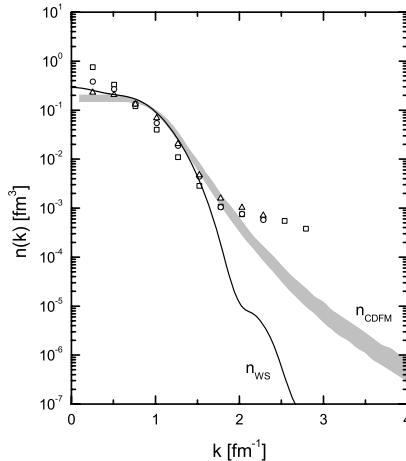
Figure: Nucleon momentum distribution $n(k)$ from: i) CDFM results for ^{4}He, ^{12}C, ^{27}Al, ^{56}Fe and ^{197}Au are combined by shaded area (n_{CDFM}); ii) "y-scaling data" given by open squares, circles and triangles for ^{4}He, ^{12}C, and ^{56}Fe, respectively; iii) mean-field calculations using Woods-Saxon single-particle wave functions for ^{56}Fe (n_{WS}).

Let's consider the basic formalism for inclusive electron scattering from nuclei in which an electron with four-momentum $\mathbf{K}^\mu = (\epsilon, \mathbf{k})$ is scattered through an angle $\theta = \angle(\mathbf{k}, \mathbf{k}')$ to four-momentum $\mathbf{K}'^\mu = (\epsilon', \mathbf{k}')$. The four-momentum transferred in the process is then $\mathbf{Q}^\mu = (\mathbf{K} - \mathbf{K}')^\mu = (\omega, \mathbf{q})$, where $\omega = \epsilon - \epsilon'$, $\mathbf{q} = |\mathbf{q}| = \mathbf{k} - \mathbf{k}'$, and $Q^2 = \omega^2 - q^2 \leq 0$. For extreme relativistic limit $|\mathbf{k}| \cong \epsilon \gg m_e$ and $|\mathbf{k}'| \cong \epsilon' \gg m_e$, where m_e is the electron mass.

In the one-photon-exchange approximation, the double-differential cross section in the laboratory system can be written in the form

$$\frac{d^2\sigma}{d\Omega d\epsilon'} = \sigma_M \left\{ \left(\frac{Q^2}{q^2} \right)^2 R_L(q, \omega) + \left[\frac{1}{2} \left| \frac{Q^2}{q^2} \right| + \tan^2 \frac{\theta}{2} \right] R_T(q, \omega) \right\}, \quad (1)$$

where L (T) refer to responses with longitudinal (transverse) projections (i.e., with respect to the momentum transfer direction) of the nuclear currents, and where the Mott cross section is given by $\sigma_M = \left[\dfrac{\alpha \cos(\theta/2)}{2\varepsilon \sin^2(\theta/2)} \right]^2$, where α the fine-structure constant.

This cross section is obtained by contracting leptonic and hadronic current-current interaction electromagnetic tensors and so is proportional to $\eta_{\mu\nu}W^{\mu\nu}$. The leptonic tensor may be calculated in the standard way involving traces of Dirac γ matrices, yielding

$$\eta_{\mu\nu} = \mathbf{K}_\mu \mathbf{K}'_\nu + \mathbf{K}'_\mu \mathbf{K}_\nu - g_{\mu\nu}\mathbf{K}\cdot\mathbf{K}' \qquad (2)$$

Contracting this with a general hadronic tensor $W^{\mu\nu}$ and rewriting the cross section in Eq. (1), we have the following for the two response functions (summation convention on repeated indices):

$$R_L(q,w) = W^{00} \text{and } R_T(q,w) = -\left(g_{ij} + \frac{q_i q_j}{q^2}\right)W^{ij} \qquad (3)$$

Hadronic tensor in the RFG model can be expressed:

$$W^{\mu\nu} = \frac{3\mathcal{N}m_N^2}{4\pi p_F^3}\int \frac{d^3p}{E(\mathbf{p})E(\mathbf{p}+\mathbf{q})}\theta(p_F - |\mathbf{p}|)\theta(|\mathbf{p}+\mathbf{q}| - p_F) \times$$
$$\times \delta[\omega - [E(\mathbf{p}+\mathbf{q}) - E(\mathbf{p})]]f^{\mu\nu}(P+Q,P), \quad (4)$$

where $f^{\mu\nu}(P+Q,P)$ is the single-nucleon response tensor obtained by Lorentz transforming the measured response involving the system where the struck nucleon is at rest to the system where the struck nucleon has four-momentum P:

$$f^{\mu\nu}(P+Q,P) = -W_1(\tau)\left(g^{\mu\nu} - \frac{Q^\mu Q^\nu}{Q^2}\right) +$$
$$+ W_2(\tau)\frac{1}{m_N^2}\left(P^\mu - \frac{P.Q}{Q^2}Q^\mu\right)\left(P^\nu - \frac{P.Q}{Q^2}Q^\nu\right) \quad (5)$$

Response functions in the RFG model can be written:

$$R_{L,T} = \frac{3\mathcal{N}}{4m_N\kappa\eta_F^3}(\varepsilon_F - \Gamma)\Theta(\varepsilon_F - \Gamma)\times$$
$$\times \begin{cases} \frac{\kappa^2}{\tau}\left[(1+\tau)W_2(\tau) - W_1(\tau) + W_2(\tau)\Delta\right] \text{ for } L \\ [2W_1(\tau) + W_2(\tau)\Delta] \text{ for } T \end{cases}, \quad (6)$$

where

$$W_1(\tau) = \tau G_M^2(\tau), \ W_2(\tau) = \frac{1}{1+\tau}[G_E^2(\tau) + \tau G_M^2(\tau)] \tag{7}$$

$$\kappa = q/2m_N, \ \lambda = \omega/2m_N, \ \tau = \kappa^2 - \lambda^2,$$
$$\eta \equiv |\mathbf{p}|/m_N, \ \varepsilon \equiv E(\mathbf{p})/m_N = \sqrt{1+\eta^2},$$
$$\eta_F \equiv p_F/m_N, \ \varepsilon_F = \sqrt{1+\eta_F^2} \tag{8}$$

$$\Delta = \frac{\tau}{\kappa^2}\left[\frac{1}{3}(\varepsilon_F^2 + \varepsilon_F\Gamma + \Gamma^2) + \lambda(\varepsilon_F + \Gamma) + \lambda^2\right] - (1+\tau),$$
$$\Gamma \equiv \max\left[(\varepsilon_F - 2\lambda), \gamma_- \equiv \kappa\sqrt{1+\frac{1}{\tau}} - \lambda\right]. \tag{9}$$

Scaling variable ψ is defined by

$$\psi \equiv \frac{1}{\sqrt{\xi_F}} \frac{\lambda - \tau}{\sqrt{(1+\lambda)\tau + \kappa\sqrt{\tau(1+\tau)}}}. \tag{10}$$

We introduce the modified CDFM approach on the basis of the RFG model for the hadronic tensor and the response functions. In CDFM:

$$\eta_F(x) = \frac{k_F(x)}{m_N} = \frac{\alpha}{x m_N}, \ \varepsilon_F(x) = \sqrt{1 + \eta_F^2(x)} = \sqrt{1 + \left(\frac{\alpha}{x m_N}\right)^2} \quad (11)$$

Responses with transverse projections for neutrons:

$$R_{T,n}(x, \psi) = \frac{3N}{4 m_N \kappa \eta_F^3(x)} (\varepsilon_F(x) - \Gamma(x)) \Theta(\varepsilon_F(x) - \Gamma(x)) \times \\ \times [2W_{1,n}(\tau) + W_{2,n}(\tau) \Delta(x, \psi)], \quad (12)$$

Responses with transverse projections for protons:

$$R_{T,p}(x, \psi) = \frac{3Z}{4 m_N \kappa \eta_F^3(x)} (\varepsilon_F(x) - \Gamma(x)) \Theta(\varepsilon_F(x) - \Gamma(x)) \times \\ \times [2W_{1,p}(\tau) + W_{2,p}(\tau) \Delta(x, \psi)], \quad (13)$$

Responses with longitudinal projections for neutrons:

$$R_{L,n}(x,\psi) = \frac{3N}{4m_N\kappa\eta_F^3(x)}(\varepsilon_F(x) - \Gamma(x))\Theta(\varepsilon_F(x) - \Gamma(x))\times$$
$$\times\frac{\kappa^2}{\tau}\left[(1+\tau)W_{2,n}(\tau) - W_{1,n}(\tau) + W_{2,n}(\tau)\Delta(x,\psi)\right], \quad (14)$$

Responses with longitudinal projections for protons:

$$R_{L,p}(x,\psi) = \frac{3Z}{4m_N\kappa\eta_F^3(x)}(\varepsilon_F(x) - \Gamma(x))\Theta(\varepsilon_F(x) - \Gamma(x))\times$$
$$\times\frac{\kappa^2}{\tau}\left[(1+\tau)W_{2,p}(\tau) - W_{1,p}(\tau) + W_{2,p}(\tau)\Delta(x,\psi)\right], \quad (15)$$

where

$$\Delta(x,\psi) = \frac{\tau}{\kappa^2}\left[\frac{1}{3}(\varepsilon_F^2(x) + \varepsilon_F(x)\Gamma(x) + \Gamma^2(x)) + \right.$$
$$\left. + \lambda(\varepsilon_F(x) + \Gamma(x)) + \lambda^2\right] - (1+\tau) \quad (16)$$

with

$$\Gamma(x) \equiv \max\left[(\varepsilon_F(x) - 2\lambda), \gamma_- \equiv \kappa\sqrt{1 + \frac{1}{\tau}} - \lambda\right] \qquad (17)$$

and

$$W_{1,p}(\tau) = \tau G_{M,p}^2(\tau) \qquad (18)$$

$$W_{1,n}(\tau) = \tau G_{M,n}^2(\tau) \qquad (19)$$

$$W_{2,p}(\tau) = \frac{1}{1 + \tau}\left[G_{E,p}^2(\tau) + \tau G_{M,p}^2(\tau)\right] \qquad (20)$$

$$W_{2,n}(\tau) = \frac{1}{1 + \tau}\left[G_{E,n}^2(\tau) + \tau G_{M,n}^2(\tau)\right]. \qquad (21)$$

Responses with longitudinal projections:

$$R_L(x, \psi) = R_{L,p}(x, \psi) + R_{L,n}(x, \psi) \Rightarrow \qquad (22)$$

$$R_L(\psi) = \int_0^\infty R_L(x, \psi)|F(x)|^2 dx. \qquad (23)$$

Responses with transverse projections:

$$R_T(x, \psi) = R_{T,p}(x, \psi) + R_{T,n}(x, \psi) \Rightarrow \quad (24)$$

$$R_T(\psi) = \int\limits_0^\infty R_T(x, \psi) |F(x)|^2 dx \quad (25)$$

We label $\dfrac{d^2\sigma}{d\Omega d\varepsilon'}$ by $C^{\text{CDFM}}(\psi)$:

$$C^{\text{CDFM}}(\psi) \equiv \frac{d^2\sigma}{d\Omega d\varepsilon'} =$$
$$= \sigma_M \left\{ \left(\frac{Q^2}{q^2}\right)^2 R_L(\psi) + \left[\frac{1}{2}\left|\frac{Q^2}{q^2}\right| + \tan^2\frac{\theta}{2}\right] R_T(\psi) \right\} \quad (26)$$

Single-nucleon eN elastic cross section:

$$S^{\text{QE}} = \sigma_M \left\{ \left(\frac{Q^2}{q^2}\right)^2 G_L^{\text{QE}}(\tau) + \left[\frac{1}{2}\left|\frac{Q^2}{q^2}\right| + \tan^2\frac{\theta}{2}\right] G_T^{\text{QE}}(\tau) \right\}, (27)$$

where single-nucleon functions G_L and G_T are given by:

$$G_L^{\text{QE}}(\tau) = \frac{\kappa}{2\tau}[ZG_{E,p}^2(\tau) + NG_{E,n}^2(\tau)] + \mathcal{O}(\eta_F^2) \tag{28}$$

$$G_T^{\text{QE}}(\tau) = \frac{\tau}{\kappa}[ZG_{M,p}^2(\tau) + NG_{M,n}^2(\tau)] + \mathcal{O}(\eta_F^2). \tag{29}$$

Superscaling function is evaluated by

$$f_{\text{CDFM}}(\psi) = k_F \times \frac{C^{\text{CDFM}}(\psi)}{S^{\text{QE}}}, \tag{30}$$

and longitudinal L and transverse T scaling functions are introduced:

$$f_L(\psi) = k_F \times \frac{R_L(\psi)}{G_L^{\text{QE}}}, \tag{31}$$

$$f_T(\psi) = k_F \times \frac{R_T(\psi)}{G_T^{\text{QE}}}. \tag{32}$$
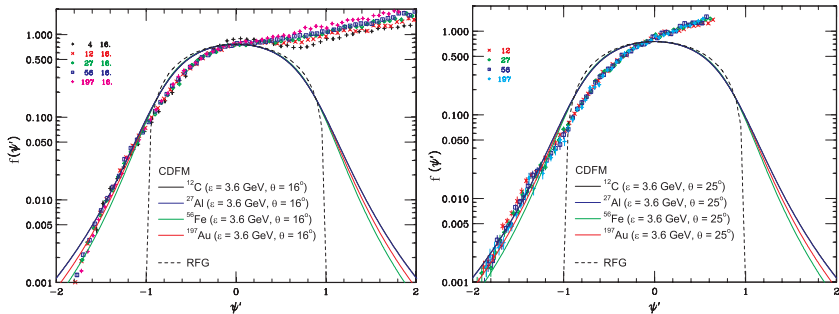
Figure: The quasielastic scaling function $f^{QE}(\psi')$ for ^{12}C, ^{27}Al, ^{56}Fe, and ^{197}Au calculated in the CDFM$_I$.
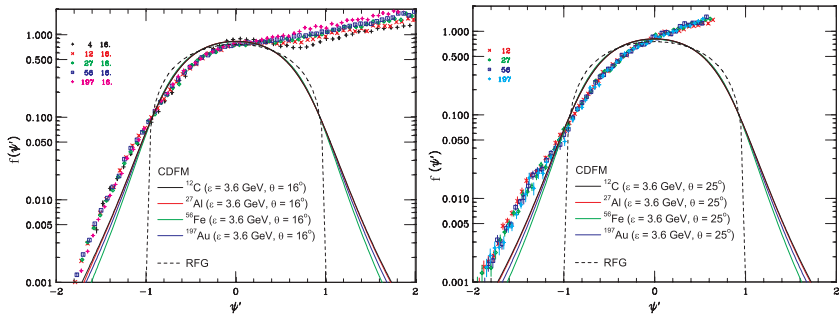
Figure: The quasielastic scaling function $f^{QE}(\psi')$ for ^{12}C, ^{27}Al, ^{56}Fe, and ^{197}Au calculated in the CDFM$_{II}$.
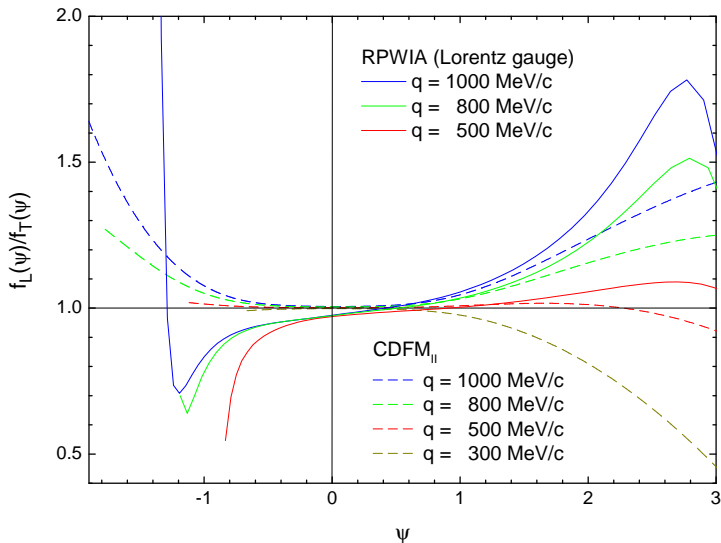
Figure: The ratio $f_L(\psi)/f_T(\psi)$ for ^{12}C calculated in the CDFM$_{II}$ and RPWIA (Lorentz gauge) for $q = 300$, 500, 800, and 1000 MeV/c.
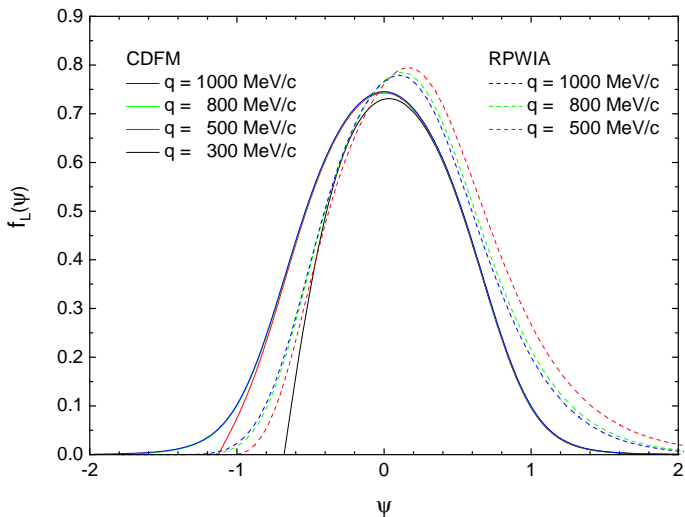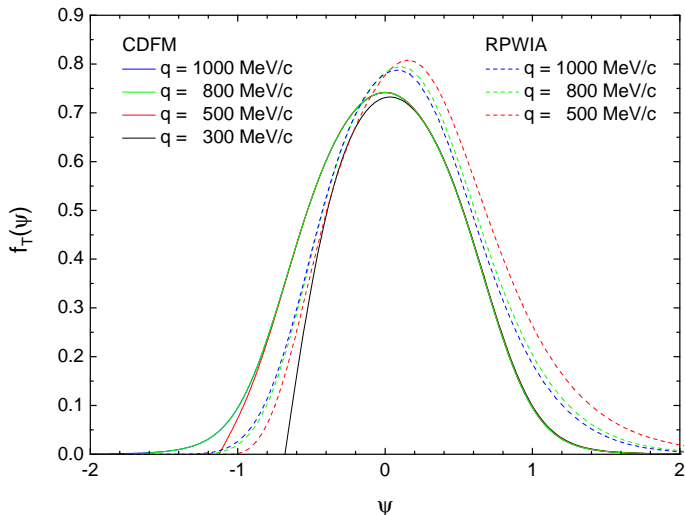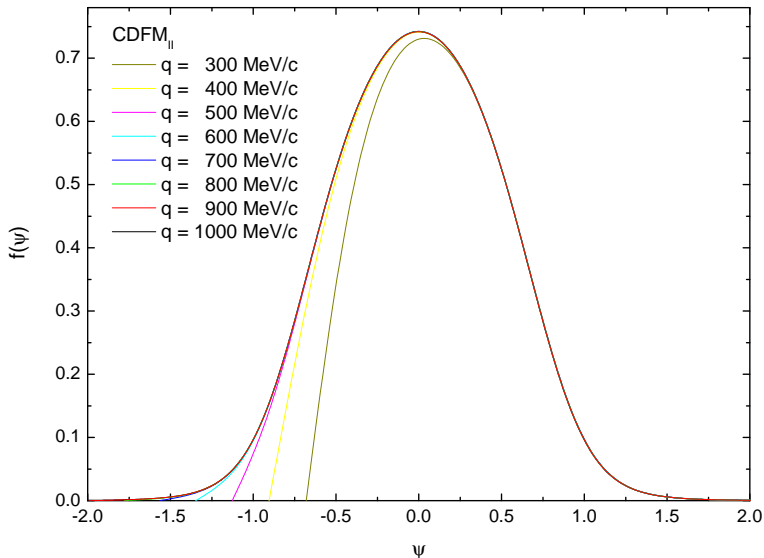
Figure: The differences $f_T(\psi) - f_L(\psi)$ for ^{12}C calculated in the CDFM$_{\parallel}$ and RPWIA (Lorentz gauge) for $q = 300$, 500, 800, and 1000 MeV/c.

Figure: The longitudinal scaling function $f_L(\psi)$ for ^{12}C calculated in the CDFM$_{II}$ and RPWIA (Lorentz gauge) for $q = 300$, 500, 800, and 1000 MeV/c.

Figure: The transverse scaling function $f_T(\psi)$ for ^{12}C calculated in the $CDFM_{II}$ and RPWIA (Lorentz gauge) for $q = 300$, 500, 800, and 1000 MeV/c.

Figure: The quasielastic scaling function $f^{QE}(\psi)$ for ^{12}C calculated in the CDFM$_{II}$ for $q = 300 - 1000$ MeV/c with step 100 MeV/c .

Dividing the cross section by the appropriate single-nucleon cross section, for $N \longrightarrow \Delta$ transition, and displaying the results versus a new scaling variable (ψ'_Δ) it is obtained that the results scale quite well.

The shifted dimensionless scaling variable in the Δ-region ψ'_Δ is introduced by the expression:

$$\psi'_\Delta \equiv \left[\frac{1}{\xi_F} \left(\kappa \sqrt{{\rho'_\Delta}^2 + \frac{1}{\tau'}} - \lambda' \rho'_\Delta - 1 \right) \right]^{1/2} \times \begin{cases} +1, & \lambda' \geq {\lambda'}^0_\Delta \\ -1, & \lambda' \leq {\lambda'}^0_\Delta \end{cases}, \quad (1)$$

where

$$\xi_F \equiv \sqrt{1 + \eta_F^2} - 1, \ \eta_F \equiv \frac{k_F}{m_N}, \ \lambda' = \lambda - \frac{E_{shift}}{2m_N},$$

$$\tau' = \kappa^2 - {\lambda'}^2, \ \lambda = \frac{\omega}{2m_N}, \ \kappa = \frac{q}{2m_N}, \ \tau = \kappa^2 - \lambda^2,$$

$${\lambda'}^0_\Delta = \lambda^0_\Delta - \frac{E_{shift}}{2m_N}, \ \lambda^0_\Delta = \frac{1}{2} \left[\sqrt{\mu_\Delta^2 + 4\kappa^2} - 1 \right], \ \mu_\Delta = \frac{m_\Delta}{m_N},$$

$$\rho_\Delta = 1 + \frac{\beta_\Delta}{\tau}, \ \rho'_\Delta = 1 + \frac{\beta_\Delta}{\tau'}, \ \beta_\Delta = \frac{1}{4} \left(\mu_\Delta^2 - 1 \right).$$

The relativistic Fermi gas superscaling function in the Δ domain is given by

$$f^\Delta_{RFG}(\psi'_\Delta) = \frac{3}{4}(1 - {\psi'_\Delta}^2)\theta(1 - {\psi'_\Delta}^2) \qquad (2)$$

Following the CDFM application to the scaling phenomenon, the Δ-scaling function in the model can be expressed:

$$f^\Delta(\psi'_\Delta) = \int_0^\infty dR |F_\Delta(R)|^2 f^\Delta_{RFG}(\psi'_\Delta(R)), \qquad (3)$$

$${\psi'_\Delta}^2(R) = \frac{\left[\kappa\sqrt{{\rho'_\Delta}^2 + \dfrac{1}{\tau'}} - \lambda'\rho'_\Delta - 1\right]}{\left[\sqrt{1 + \dfrac{k_F^2(R)}{m_N^2}} - 1\right]} \equiv t(R).{\psi'_\Delta}^2, \qquad (4)$$

$$t(R) \equiv \left[\sqrt{1 + \frac{k_F^2}{m_N^2}} - 1\right] \Big/ \left[\sqrt{1 + \frac{k_F^2(R)}{m_N^2}} - 1\right] \text{ and } k_F(R) = \frac{\alpha}{R}. \quad (5)$$

It was shown that though the functional forms of $f^\Delta(\psi'_\Delta)$ and the weight function $|F_\Delta(R)|^2$ are like in the QE region, the parameters of the densities (e.g. the half-radius R_Δ and the diffuseness b_Δ when Fermi-type distributions have been used) may be different from R and b in the QE case.

Fitting the scaling data of the Δ peak extracted from the high-quality world data for inclusive electron scattering, we found for ^{12}C the values $R_\Delta = 1.565$ fm and $b_\Delta = 0.420$ fm and a coefficient in the right-hand side of Eq. (2) for the RFG scaling function $f^\Delta_{\mathrm{RFG}}(\psi'_\Delta)$ equal to 0.54 instead of $3/4$. (The Fermi momentum was taken to be $k_F = 1.20$ fm^{-1} and this choice leads to normalization to unity of $f^\Delta_{\mathrm{RFG}}(\psi'_\Delta)$.)

The value of R_Δ is smaller than that used in the description of the QE superscaling function for ^{12}C ($R = 2.470$ fm), whereas the value of b_Δ is the same as b in the QE case.
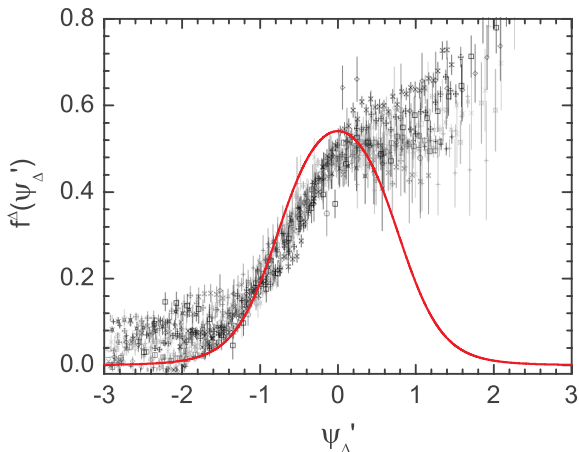
Figure: The CDFM scaling function $f^{\Delta}(\psi'_{\Delta})$ in the Δ-region (solid red line). Averaged experimental values of $f^{\Delta}(\psi'_{\Delta})$ are taken from:
J. E. Amaro, M. B. Barbaro, J. A. Caballero, T. W. Donnelly, A. Molinari, and I. Sick, *Phys. Rev. C* **71**, 015501 (2005).
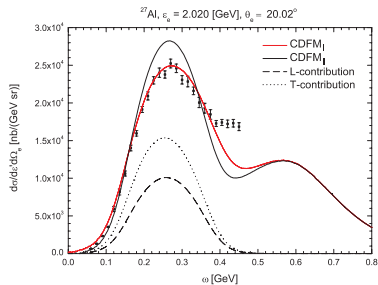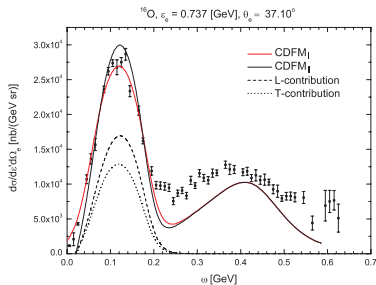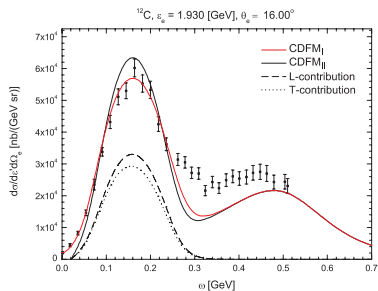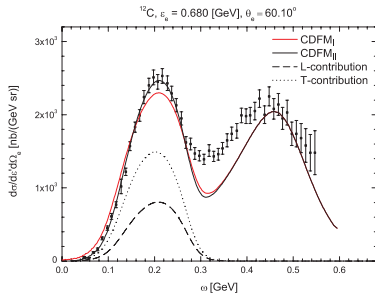
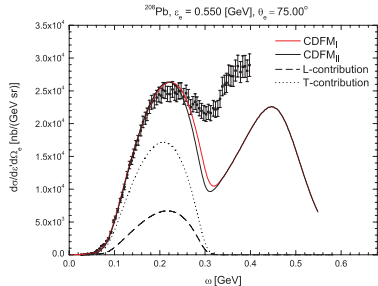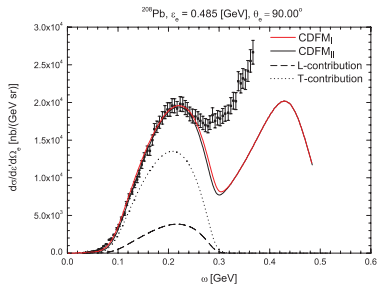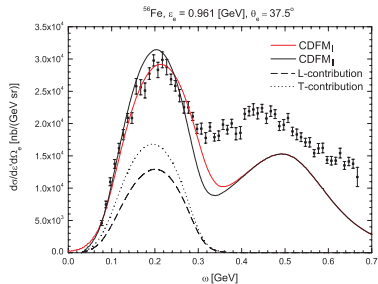Figure: Inclusive electron cross sections as function of energy loss.

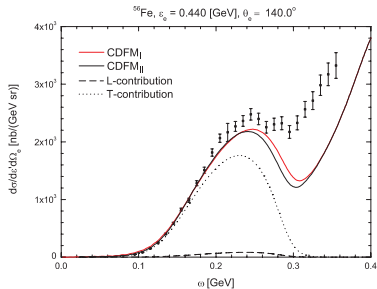Figure: Inclusive electron cross sections as function of energy loss.

– Following:

📄 J. E. Amaro, M. B. Barbaro, J. A. Caballero, T. W. Donnelly, A. Molinari, and I. Sick, *Phys. Rev. C* **71**, 015501 (2005).

the CC neutrino cross section in the target laboratory frame is given in the form

$$\left[\frac{d^2\sigma}{d\Omega dk'}\right]_\chi \equiv \sigma_0 \mathcal{F}_\chi^2, \tag{1}$$

where $\chi = +$ for neutrino-induced reactions (for example, $\nu_l + n \to \ell^- + p$, where $\ell = e, \mu, \tau$) and $\chi = -$ for antineutrino-induced reactions (for example, $\overline{\nu_l} + p \to \ell^+ + n$),

$$\sigma_0 \equiv \frac{(G\cos\theta_c)^2}{2\pi^2}\left[k'\cos\widetilde{\theta}/2\right]^2, \tag{2}$$

where $G = 1.16639 \times 10^{-5}$ GeV^{-2} is the Fermi constant, θ_c is the Cabibbo angle ($\cos\theta_c = 0.9741$),

$$\tan^2\widetilde{\theta}/2 \equiv \frac{|Q^2|}{v_0}, \tag{3}$$

$$v_0 \equiv (\epsilon + \epsilon')^2 - q^2 = 4\epsilon\epsilon' - |Q^2|. \qquad (4)$$

The function $\mathcal{F}_\chi^2$ depends on the nuclear structure and is presented as a generalized Rosenbluth decomposition having charge-charge, charge-longitudinal, longitudinal-longitudinal and two types of transverse responses.

The nuclear response functions in both QE- and Δ-regions are expressed in terms of the nuclear tensor $W^{\mu\nu}$ in the corresponding region, using its relationships with the RFG model scaling functions. This concerns the leptonic and hadronic tensors and the response and structure functions.

Instead of the RFG functions in the QE and Δ regions, we use those obtained in the CDFM.
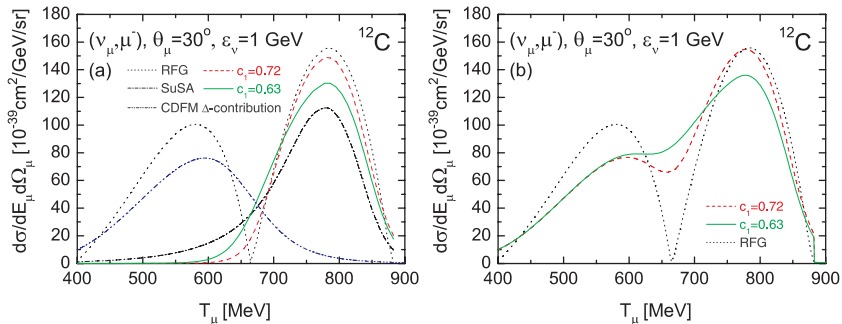
Figure: The cross section of charge-changing neutrino (ν_μ, μ^-) reaction on ^{12}C at $\theta_\mu = 30^\circ$ and $\varepsilon_\nu = 1$ GeV. (a) QE contributions: solid line: the result of CDFM with $c_1 = 0.63$; dashed line: CDFM with $c_1 = 0.72$; dotted line: RFG; dot-dashed line: SuSA result; double dot-dashed line: the result for the Δ-contribution from the CDFM. (b) the sum of QE- and Δ-contributions in RFG model (dotted line), in the CDFM with $c_1 = 0.63$ (solid line) and $c_1 = 0.72$ (dashed line).
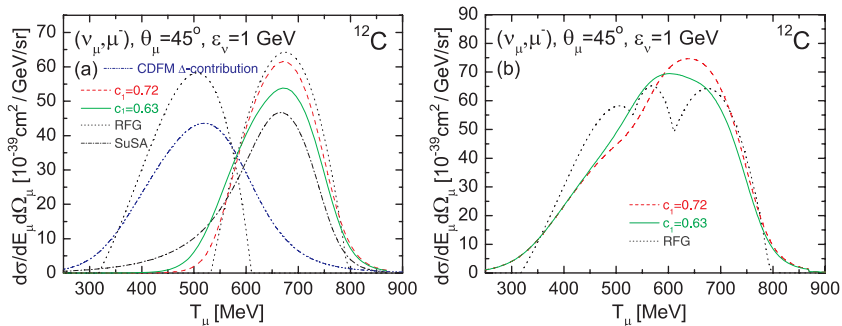
Figure: The cross section of charge-changing neutrino (ν_μ, μ^-) reaction on ^{12}C at $\theta_\mu = 45°$ and $\varepsilon_\nu = 1$ GeV.

Figure: The cross section of charge-changing neutrino (ν_μ, μ^-) reaction on ^{12}C at $\theta_\mu = 60°$ and $\varepsilon_\nu = 1$ GeV.

Figure: The cross section of charge-changing neutrino (ν_μ, μ^-) reaction on ^{12}C at $\theta_\mu = 45°$ and $\varepsilon_\nu = 1$ GeV.
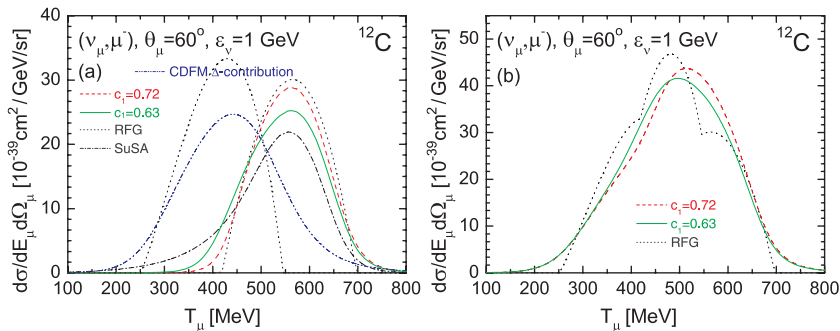
Figure: The cross section of charge-changing neutrino (ν_μ, μ^-) reaction on ^{12}C at $\theta_\mu = 45°$ and $\varepsilon_\nu = 1.5$ GeV.

Figure: The cross section of charge-changing neutrino (ν_μ,μ^-) reaction on ^{12}C at $\theta_\mu = 45°$ and $\varepsilon_\nu = 2$ GeV.

Figure: The cross section of charge-changing antineutrino $(\overline{\nu}_\mu, \mu^+)$ reaction on ^{12}C at $\theta_\mu = 45°$ and $\varepsilon_{\overline{\nu}} = 1$ GeV.

Figure: The cross section of charge-changing neutrino (ν_μ, μ^-) reaction on ^{12}C at $\theta_\mu = 45°$ and $\varepsilon_\nu = 1$ GeV.
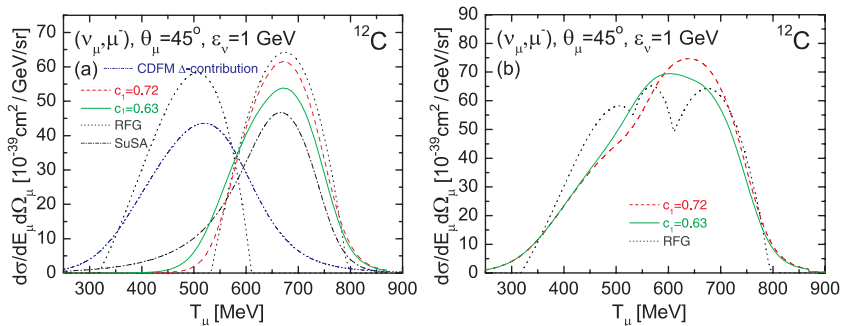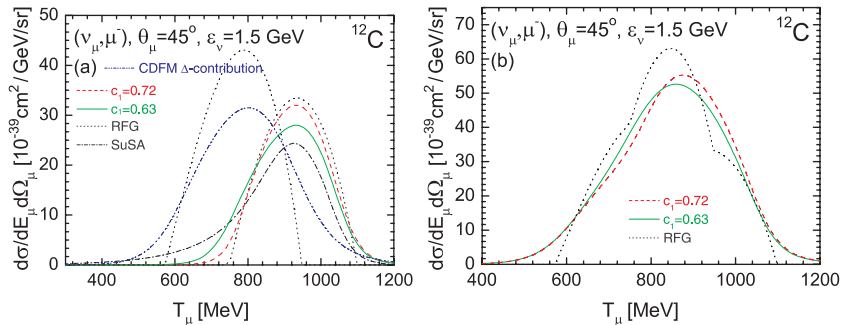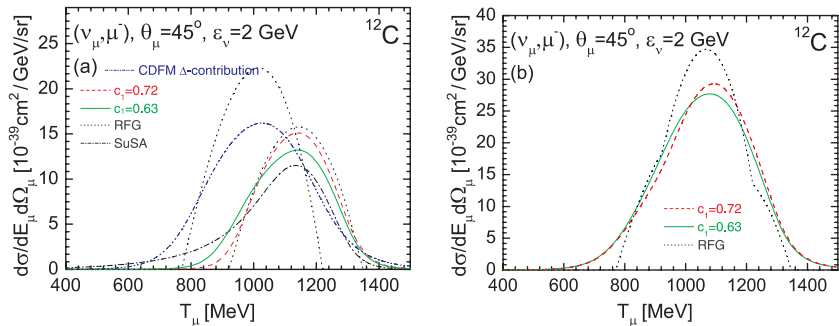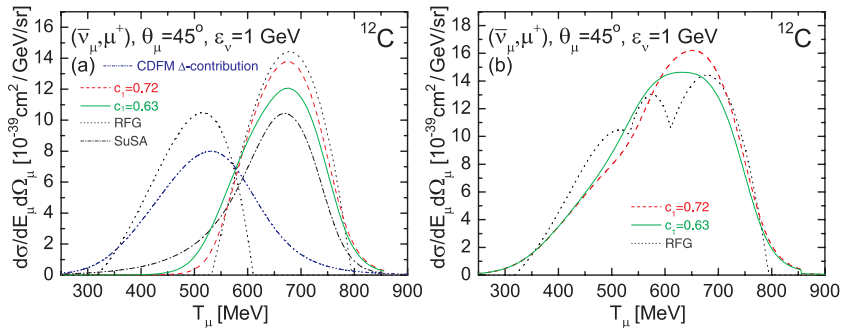
Discussions:
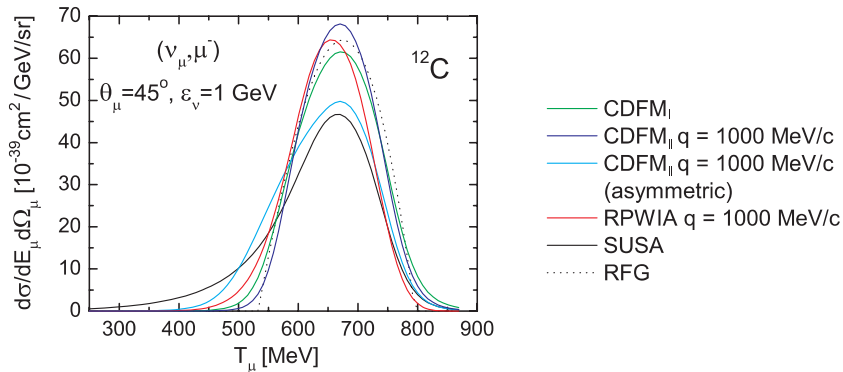
- The use of asymmetric CDFM scaling function ($c_1 = 0.63$) gives results which are close to those from SuSA, while the symmetric scaling function ($c_1 = 0.72$) leads to results similar with the RFG model ones.
- At fixed incident energies the values of the QE- and Δ-peak maxima decrease with the increase of the muon angle θ_μ and the value of the Δ-contribution maximum becomes closer to that of the QE contribution.
- At fixed angle θ_μ the QE- and Δ-contributions overlap more strongly with the increase of the neutrino energy and the maximum of the Δ-peak increases with respect to the QE peak.
- At fixed angle θ_μ the maximum of the sum of both QE- and Δ-contributions to the cross section decrease with the increase of the energy. For $\theta_\mu = 45°$ both CDFM curves (with $c_1 = 0.63$ and $c_1 = 0.72$) are quite similar for the interval of neutrino energies $\varepsilon_\nu = 1 \div 2$ GeV.

- At energy $\varepsilon_\nu = 1$ GeV and smaller angles (*e.g.* $\theta_\mu = 30°$) there are two maxima of the total sum of the QE- and Δ-contributions, while at larger angles ($\theta_\mu = 45°$ and $60°$) the two peaks merge into one (for the energy interval $\varepsilon_\nu = 1 \div 2$ GeV).
- The antineutrino cross section (on the example for incident energy 1 GeV and muon angle of 45 degrees) is about 5 times smaller than the neutrino one.

A.N. Antonov, M.V. Ivanov, M.K. Gaidarov, E.Moya de Guerra, J.A. Caballero, M.B. Barbaro, J.M. Udias, P. Sarriguren, "Superscaling analysis of inclusive electron scattering and its extension to charge-changing neutrino-nucleus cross sections beyond the relativistic Fermi gas approach", *Phys. Rev. C* **74**, 054603 (2006).

M.V. Ivanov, M.B. Barbaro, J.A. Caballero, A.N. Antonov, E. Moya de Guerra, M.K. Gaidarov, "Superscaling and charge-changing neutrino scattering from nuclei in the Δ region beyond the relativistic Fermi gas model", *Phys. Rev. C* **77**, 034612 (2008).

We consider the semi-leptonic quasi-free scattering from nuclei in Born approximation, assuming that the inclusive cross sections are well represented by the sum of the integrated semi-inclusive proton and neutron emission cross sections.

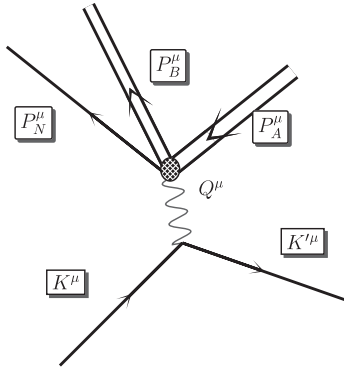Figure: The kinematics for semi-leptonic nucleon knockout reactions in the one-boson-exchange approximation.

A lepton with 4-momentum $K^\mu = (\epsilon, \mathbf{k})$ scatters to another lepton with 4-momentum $K'^\mu = (\epsilon', \mathbf{k}')$, exchanging a vector boson with 4-momentum $Q^\mu = K^\mu - K'^\mu$.

$$\epsilon = \sqrt{m^2 + k^2}, \; \epsilon' = \sqrt{m'^2 + k'^2} \quad (1)$$
$$m \cong 0, \; m' \cong 0$$

In the laboratory system

- The initial nucleus has a 4-momentum – $P_A^\mu = (M_A^0, 0)$

Final hadronic state corresponds to:

- a proton or neutron with 4-momentum $P_{N=p \text{ or } n}^\mu = (E_N, \mathbf{p}_N)$
- an unobserved residual nucleus with 4-momentum $P_B^\mu = (E_B, \mathbf{p}_B)$

$$\mathbf{p} \equiv -\mathbf{p}_B \text{ – the missing momentum;}$$

$$\mathcal{E} \equiv E_B - E_B^0 \text{ – the excitation energy; } E_B^0 = \sqrt{\left(M_B^0\right)^2 + p^2}$$

$$M_B^0 \text{ – the ground-state mass of the daughter nucleus}$$

$$Q'^\mu \equiv K^\mu - P_N^\mu = (\omega', \mathbf{q}') \text{– 4-momentum in the } u\text{-channel}$$

$$q' = |\mathbf{q}'| = \sqrt{k^2 + p_N^2 - 2kp_N \cos\theta_{kp_N}}$$

Following procedure for calculating the inclusive cross section in the *u*-channel from work:

📄 J. E. Amaro, M. B. Barbaro, J. A. Caballero, and T. W. Donnelly, Phys. Rev. C **73**, 035503 (2006) – SuperScaling Analysis (SuSA).

after some approximations cross section can be written in the form:

$$\frac{d\sigma}{d\Omega_N dp_N} \simeq \overline{\sigma}_{sn}^{(u)} F(y', q'), \qquad (2)$$

$$F(y', q') \equiv \int\limits_{\mathcal{D}_u} p dp \int \frac{d\mathcal{E}}{E} \Sigma \simeq F(y'), \qquad (3)$$

$$\overline{\sigma}_{sn}^{(u)} = \frac{1}{32\pi\epsilon} \frac{1}{q'} \left(\frac{p_N^2}{E_N}\right) g^4 \int\limits_0^{2\pi} \frac{d\phi'}{2\pi} l_{\mu\nu}(\mathbf{k}, \mathbf{k}') w^{\mu\nu}(\mathbf{p}, \mathbf{p}_N) D_V(Q^2)^2 \qquad (4)$$

effective neutral current single nucleon cross section

In Eq. (4) $l_{\mu\nu}$ and $w^{\mu\nu}$ are the leptonic and s.n. hadronic tensor, respectively, and $D_V(Q^2)$ is the vector boson propagator. In Eq. (2) y' is the scaling variable naturally arising in the u-scattering kinematics, analogous to the usual y-scaling variable for t-scattering. The scaling function $F(y')$ obtained within a given approach can be used to predict realistic NC cross sections. The RFG u-channel ψ-variable is introduced in the form:

$$\psi_{RFG}^{(u)} = s\sqrt{\frac{m_N}{T_F}} \left[\sqrt{1 + \left(\frac{y_{RFG}^{(u)}}{m_N}\right)^2} - 1 \right]^{1/2}, \qquad (5)$$

where

$$y_{RFG}^{(u)} = s\frac{m_N}{\tau'} \left[\lambda'\sqrt{\tau'^2\rho'^2 + \tau'} - \kappa'\tau'\rho' \right] \qquad (6)$$

is the RFG y-scaling variable for the u-channel and corresponds to the minimum momentum required for a nucleon to participate in the NC neutrino-nucleus scattering.

The dimensionless kinematic quantities in Eq. (6) are given by: $\kappa' \equiv q'/2m_N$, $\lambda' \equiv \omega'/2m_N$, $\tau' = \kappa'^2 - \lambda'^2$ and defined $\rho' \equiv 1 - \dfrac{1}{4\tau'}(1 - m'^2/m_N^2)$. The sign s is

$$s \equiv \text{sgn} \left\{ \frac{1}{\tau'} \left[\lambda' \sqrt{\tau'^2 \rho'^2 + \tau'} - \kappa' \tau' \rho' \right] \right\}. \qquad (7)$$

The physical meaning of $\psi_{\text{RFG}}^{(u)2}$ is the minimum kinetic energy of the nucleon participating in the reaction. The RFG scaling function is found to be:

$$F_{\text{RFG}}(\psi_{\text{RFG}}^{(u)}) = \frac{3}{4} k_F \left(1 - \psi_{\text{RFG}}^{(u)2} \right) \Theta \left(1 - \psi_{\text{RFG}}^{(u)2} \right). \qquad (8)$$
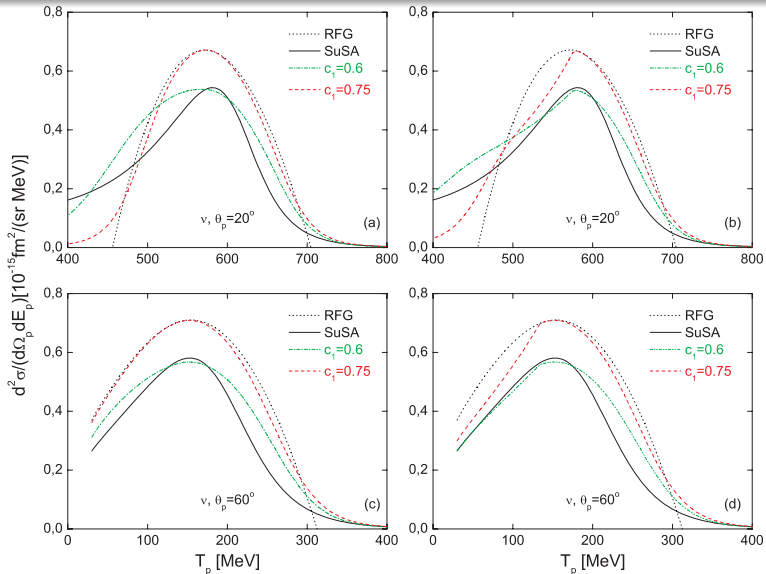
Figure: Quasielastic differential cross section for neutral current neutrino scattering at 1 GeV from ^{12}C for proton knockout at $\theta_p = 20°$ (a,b) and $60°$ (c,d).
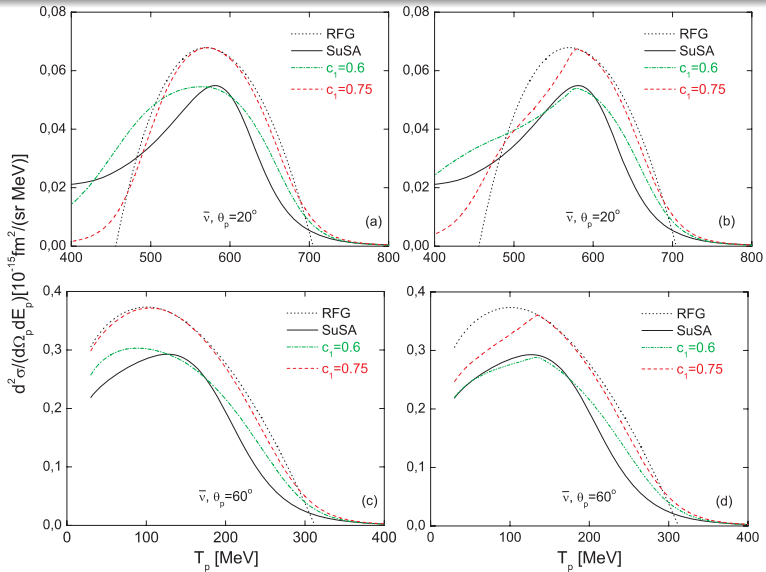
Figure: Quasielastic differential cross section for neutral current antineutrino scattering at 1 GeV from ^{12}C for proton knockout.
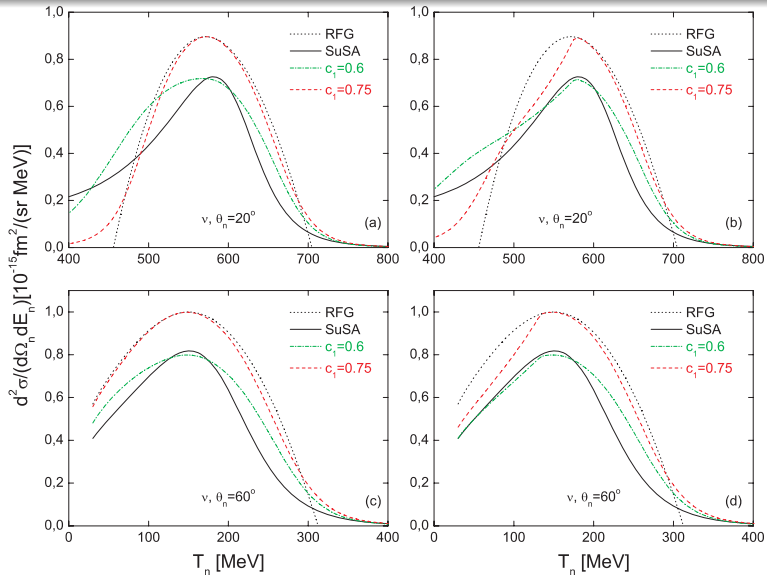
Figure: Quasielastic differential cross section for neutral current neutrino scattering at 1 GeV from ^{12}C for neutron knockout.
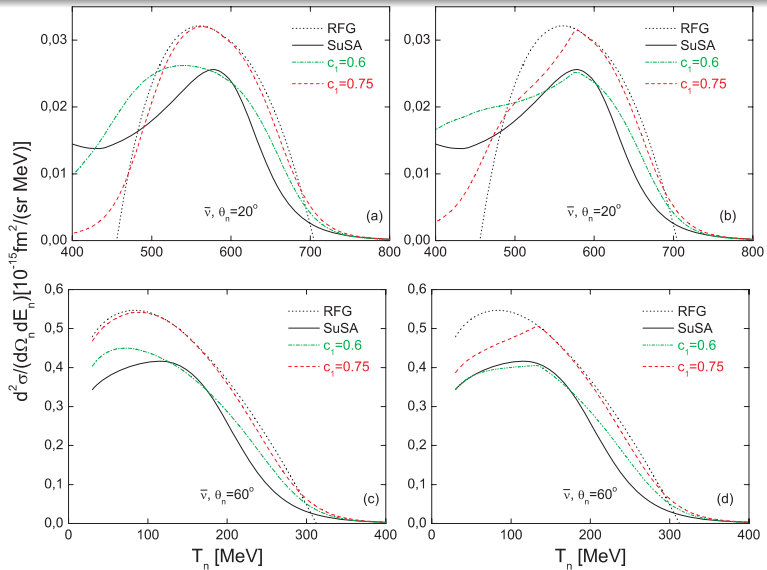
Figure: Quasielastic differential cross section for neutral current antineutrino scattering at 1 GeV from ^{12}C for neutron knockout.

Discussions:

1. We construct two different asymmetric scaling functions within CDFM: one uses a **parabolic form** of the function at positive ψ' values, the second uses an **exponential form** of that function at $\psi' > 0$. These scaling functions have been used in the calculations of quasielastic differential cross section for neutral current neutrino scattering at 1 GeV from ^{12}C for proton and neutron knockout at $\theta_p = 20°$ and $60°$.

2. It can be seen from our results at $60°$ that the neutrino and antineutrino cross sections are roughly in a $2 : 1$ ratio. For larger scattering angle values, neutrino and antineutrino cross sections come closer, diminishing the above ratio.

   Moreover, the neutron knockout cross sections are somewhat larger than the proton knockout cross sections due to the behavior of the NC single-nucleon form factors.

3. It was shown that the use of asymmetric CDFM scaling function gives results which are close to those from SuSA, while the results with symmetric scaling function are more similarity with the RFG model results.

Discussions:

1. We construct two different asymmetric scaling functions within CDFM: one uses a **parabolic form** of the function at positive ψ' values, the second uses an **exponential form** of that function at $\psi' > 0$. These scaling functions have been used in the calculations of quasielastic differential cross section for neutral current neutrino scattering at 1 GeV from ^{12}C for proton and neutron knockout at $\theta_p = 20°$ and $60°$.

2. It can be seen from our results at $60°$ that the neutrino and antineutrino cross sections are roughly in a $2 : 1$ ratio. For larger scattering angle values, neutrino and antineutrino cross sections come closer, diminishing the above ratio.

   Moreover, the neutron knockout cross sections are somewhat larger than the proton knockout cross sections due to the behavior of the NC single-nucleon form factors.

3. It was shown that the use of asymmetric CDFM scaling function gives results which are close to those from SuSA, while the results with symmetric scaling function are more similarity with the RFG model results.

Discussions:

1. We construct two different asymmetric scaling functions within CDFM: one uses a **parabolic form** of the function at positive ψ' values, the second uses an **exponential form** of that function at $\psi' > 0$. These scaling functions have been used in the calculations of quasielastic differential cross section for neutral current neutrino scattering at 1 GeV from ^{12}C for proton and neutron knockout at $\theta_p = 20°$ and $60°$.

2. It can be seen from our results at $60°$ that the neutrino and antineutrino cross sections are roughly in a $2 : 1$ ratio. For larger scattering angle values, neutrino and antineutrino cross sections come closer, diminishing the above ratio.

   Moreover, the neutron knockout cross sections are somewhat larger than the proton knockout cross sections due to the behavior of the NC single-nucleon form factors.

3. It was shown that the use of asymmetric CDFM scaling function gives results which are close to those from SuSA, while the results with symmetric scaling function are more similarity with the RFG model results.

📄 A. N. Antonov *et al.*, "Superscaling and neutral current quasielastic neutrino-nucleus scattering beyond the relativistic Fermi gas model", *Phys. Rev. C* **75**, 064617 (2007).